博士論文（要約）

A hyperbolic-equation system approach for electron fluid calculation and its application to Hall thruster analyses

（双曲型方程式系による電子流体計算と
ホールスラスタ解析への応用）

川嶋　嶺

東京大学大学院工学系研究科
航空宇宙工学専攻

On Publication of Summary of Dissertation

To be compliant with the "Publication Guidelines for Abridged Versions of Doctorate Theses," Sec. 4.3 - 4.8 and Sec. 5.2 - 5.5 are deleted [1]. The contents in these sections are to be published in academic journals.

[1] 「博士論文の内容を要約したもの」の公表に関するガイドライン, 東京大学.

Acknowledgment

The author would first like to thank Prof. Kimiya Komurasaki for supervising the doctoral research and dissertation. He has always been guiding the author to detecting fundamental issues and solving them. He has advised the author to learn about CFD, and the author found a novelty in applying CFD techniques to anisotropic diffusion problems.

The author would also like to thank Prof. Yoshihiro Arakawa. He introduced the author to the field of numerical simulation by giving the author a topic of plasma flow simulation in a plasma processing equipment. Since then, the author has been interested in the numerical analyses of plasma flows.

Dr. Hiroyuki Koizumi, and Dr. Tony Schönherr has provided a lot of invaluable comments in laboratory seminars. Owing to these advises, the author has found new perspectives on the research.

The author would also like to thank Prof. Kojiro Suzuki, Prof. Takehiro Himeno, Prof. Ikkoh Funaki for many informative comments in completing this research.

The beneficial discussions on numerical analyses with Dr. Shinatora Cho, Mr. Shohei Akagi, and Mr. Kazuki Uemoto accelerates the doctoral research. The discussions with other Hall thruster group members: Mr. Masaya Hosoda, Mr. Daiki Fujita, Mr. Yuki Ito, Mr. Jun Suzuki, Mr. Yuya Hirano, Mr. Junhwi Bak, help the author understand the physics of plasmas from the experimental side. The author thanks all of the laboratory members for supplying a good environment which motivates the author's research life.

Finally, I would thank Japan Society for the Promotion of Science (JSPS) for sponsoring this research by Grant-in-Aid for JSPS Fellows, No. 24-10079.

Contents

List of Figures

List of Tables

Nomenclature

a, b_x, b_y, c_x, c_y	Acceleration coefficients
B	Magnetic flux density
c_s	Acoustic velocity
D_norm	Normalized difference of variable
e	Elemental charge
E	Electric field
E_norm	Normalized error of variable
f	Velocity distribution function
f_m	Maxwellian distribution function
g	Energy diffusion speed
J	Jacobian matrix
Kn	Knudsen number
L	Channel length
m	Particle mass
n	Number density
N_cell	Number of cells

p	Pressure
Q	Heat flux
r_{L}	Larmor radius
t	Time
T	Temperature
u	Flow velocity
v	Particle speed
α	Coefficient for handling ionization, excitation, and radiation
α_{B}	Bohm diffusion coefficient
γ	Specific heat ratio
Γ	Number flux
κ	Electron heat transfer coefficient
λ	Eigenvalue
λ_{D}	Debye length
λ_{m}	Mean free path
μ	Electron mobility
ν_{col}	Total collision frequency
ν_{ion}	Ionization collision frequency
Ω_{e}	Electron Hall parameter
ϕ	Space potential
ϕ_{n}	Negative space potential

ϕ_{th}	Thermalized potential
σ_{col}	Total collision cross section
σ_{ion}	Ionization collision cross section
τ_{m}	Mean free time
θ	Angle between computational mesh and magnetic line
Θ	Rotation matrix regarding θ
ε_0	Vacuum permittivity
$\varepsilon_{\mathrm{ion}}$	First ionization energy
	Subscript and superscript
$\parallel$	(Subscript) Orthogonal direction of magnetic lines
$\perp$	(Subscript) Tangential direction of magnetic line of force
e	(Subscript) Electron
i	(Subscript) Ion
mag	(Subscript) Coordinate system fitted to magnetic lines
n	(Subscript) Neutral particle
r	(Subscript) Radial direction
s	(Subscript) Plasma sheath boundary
th	(Subscript) Thermal
w	(Subscript) Wall
z	(Subscript) Axial direction
$*$	(Superscript) Representative quantity
$\sim$	(Superscript) Normalized quantity

Chapter 1

Introduction

1.1 Plasma flow simulations

In recent years, the importance of plasma flow simulation has been increasing in many fields of science and engineering. One of the characteristics of plasma flow simulation is characteristic speeds existing in wide range. Generally plasma simulations handle ions, electrons, neutral particles, and electromagnetic field. Fig. 1-1 presents the typical characteristic speeds of elements in plasma simulations. For instance, if the time step is set to calculate the electromagnetic field time-dependently, an enormous calculation step is needed to observe the phenomena in the time-scale of neutral particles. Therefore, steady states are assumed for elements which have much high speed of information compared to the concerned phenomena.

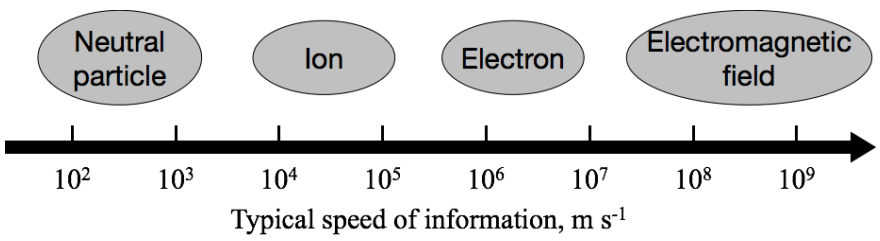

Figure 1-1: Characteristic speeds of elements (governing equations) in plasma simulations.

There has been a lot of approaches of plasma calculation for various types of plasmas. Representative models for plasmas are shown in Fig. 1-2. It is noted that the characterization in Fig. 1-2 is based on the general understanding, and the location of each model in the map subject to change in the actual codings. Several numerical models have been proposed to attain reasonable computational cost and application range suited to the simulation target.

The hybrid model applies the kinetic model for ion motions, whereas the electron flow is regarded as a fluid. This model has been adopted in many numerical simulations for various applications such as nuclear fusion,[1] space plasma,[2] and electric propulsions. In the calculations using the hybrid model, the target of interest is generally how the ions are generated and how they are accelerated. Thus, the physical phenomena in the ion time scale is concerned and the electron flow is typically assumed to be time constant. In this case, a time-constant electron density is considered, and the electron flow has a characteristics similar to those of incompressible fluid. Therefore, the conservation equations of electron fluid have been conventionally calculated with computational methods for incompressible fluid utilizing elliptic or parabolic equations.

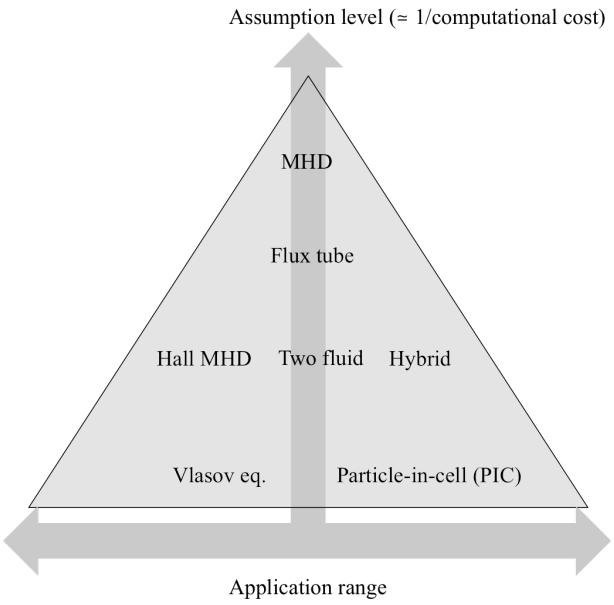

Figure 1-2: Review of various models for plasma flow simulation.

1.2 Magnetized plasma flow in Hall thrusters

Hall thrusters are promising technology for high-power electric propulsion system which enables next-generation missions such as the manned Mars mission and solar power satellite. The magnetized plasma flow in Hall thrusters can be characterized by following relations:

$$\Omega_{\mathrm{e}} \gg 1, \qquad r_{\mathrm{L,e}} \ll L \ll r_{\mathrm{L,i}}, \qquad \lambda_{\mathrm{m,e}} \ll L, \tag{1.1}$$

where Ω_{e}, $r_{\mathrm{L,e}}$, $r_{\mathrm{L,i}}$, L, and $\lambda_{\mathrm{m,e}}$ are electron Hall parameter, electron Larmor radius, ion Larmor radius, channel length, and electron mean-free path, respectively. The first relation means that the electron flow is strongly confined by the magnetic field. The second relation indicates that the finite Larmor radius effect is negligible in the electron flow, whereas the ion flow is hardly magnetized. The third relation means that the electron flow in Hall thrusters can be regarded as a collisional flow.

In the development of Hall thrusters, the important role of numerical simulations is the lifetime investigation. It is known that the factor of lifetime limitation is the channel wall erosions.[3] Since endurance tests for lifetime investigation is costly, the replacement of experiments by numerical simulations saves a lot of cost and time. A number of simulations have been conducted for the prediction of thruster lifetime[4] and reduction of wall erosions.[5] Recently a technology named "magnetic shielding" has been proposed.[6] A significant reduction of channel wall erosion was observed,[7] and the mechanism of the technology has been investigated by numerical analyses.[8] The magnetic shielding utilizes concave magnetic lines of force toward downstream, which bypass the channel wall. The future numerical simulations for Hall thrusters should be capable of two-dimensional calculations for analyzing the effect of complicated magnetic topology in the magnetic shielding. Therefore, there exists a demand of an efficient and accurate computational method for two-dimensional calculation of Hall thrusters.

1.3 Plasma modelings of Hall thruster discharge

The plasma models for Hall thruster simulations can be categorized into three models: fully kinetic, hybrid, and fully fluid models. The kinetic model is generally calculated by using the particle-in-cell (PIC) method. The characteristics of the three methods are compared in Table. 1.1. Each method is explained in detail in this section.

Table 1.1: Summary of plasma models for Hall thruster simulations.

Model	Ions, Neutrals	Electrons	Cost	Reference
Full PIC	Particle	Particle	Large	Cho,[4] Szabo[9]
Hybrid PIC	Particle	Fluid	Middle	Parra,[10] Perez-Luna[11]
Fully fluid	Fluid	Fluid	Small	Mikellides,[6] Keidar[12]

Full PIC method

The full PIC method handles ions, neutral particles, and electrons as particles. The full PIC method is able to calculate the velocity distribution function of both ions and electrons. Also, the non-neutral region like wall sheaths can also be analyzed with the full PIC method. The disadvantage of this approach is enormous computational cost. Practical codes for Hall thruster simulations using the full PIC method generally introduce artificial models to reduce the computational cost. Recent works of numerical simulations using the fully kinetic model are the ones by Cho[4] and Szabo.[9] Both of these works calculated the motions of ions, neutrals, and electrons by PIC methods, and the electric field was calculated by the Gauss's law. The feature of the Szabo's work was the use of the artificial mass ratio factor and artificial permittivity. The feature of Cho's work was the use of semi-implicit method in addition to the artificial mass ratio model.

Hybrid model

The hybrid PIC method handles ions and neutrals as particles, whereas electrons are regarded as fluid. The computational cost is significantly reduced by applying the fluid approximation to the electron flow. The motions of heavy particles are

calculated by the PIC method.

In the conventional hybrid PIC method, the magnetized electron fluid is calculated by using the so-called "quasi-one-dimensional model." The numerical simulation based on this model is originally proposed by Fife.[13] This code has been improved to include various physics and the relatively recent code is named HPHall-2.[10] The calculation processes in the quasi-one-dimensional model are illustrated in Fig. 1-3. This model assumes the isothermal property and the Boltzmann relation along the magnetic lines of force. An one-dimensional magnetic-field-aligned mesh (MFAM) which has the magnetic surfaces for mesh boundaries is prepared, and the fluxes flowing across the magnetic surfaces are integrated into the one-dimensional conservation equation. The distributions of plasma properties along the magnetic lines of force are determined based on the isothermal property and Boltzmann relation.

However, the use of the one-dimensional MFAM limits the range of application to relatively simple magnetic field geometry. The one-dimensional MFAM cannot be defined in the complicated magnetic topology, such as the ones for magnetically shielded thrusters. In order to analyze Hall thrusters with complicated magnetic topology, one needs a computational method which enables the two-dimensional calculation of magnetized electron fluid.

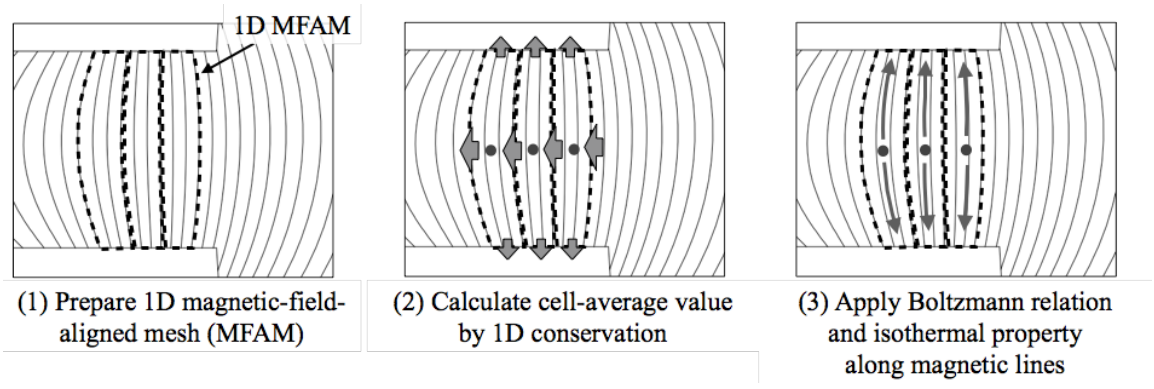

Figure 1-3: Calculation processes in the quasi-one-dimensional model.

Fully fluid model

The fully fluid model assumes fluid for ions, neutrals, and electrons. Since ions are regarded as fluid, the kinetic effects of heavy particles are neglected. The advantages of this model is the small computational cost and smooth calculation results. The computational cost is reduced by assuming fluids for both heavy particles and electrons, which enables the computation of a large calculation area.[14] A representative work of the fully fluid method is the Hall2De,[6] which has been utilized for investigating the magnetic shielding. The characteristics of this method is the use of two-dimensional magnetic-field-aligned mesh (MFAM).

However, it is controversial if the fluid model is applicable to the ion flow. In the Hall thruster plume, a deviation from the Maxwellian distribution was observed in the ion energy distribution.[15] It was reported that one factor of this deviation is related to the presence charge-exchange collisions (CEX). To permit the existence of several Maxwellian distributions of different temperatures, one needs to employ a two- or more temperature model, which degrades the simplicity of the fluid model.

1.4 Statement of issues

The characteristics of the electron fluid in Hall thrusters is the high anisotropy owing to the strong magnetic confinement. The large difference of electron mobilities between the tangential and orthogonal directions of magnetic lines of force makes the computation of the fluid difficult. If the elliptic or parabolic equations are used, these equations become anisotropic diffusion equations. Numerical instabilities arise in computing the anisotropic diffusion equation. Further, the disparity of electron mobilities causes an imbalance of information of speed in different directions, which results in a slow convergence speed. Also, it is known that the calculation suffers a large numerical diffusion if the computational mesh is not aligned with magnetic lines of force.[14,16] In order to enable the two-dimensional calculation of magnetized electron fluids, it is necessary to develop a computational method which can cope with the above issues.

1.5 MFAM-based approach and HES approach

Magnetic-field-aligned mesh (MFAM) approach

As described in the previous section, the large disparity in electron mobilities makes the computation of the magnetized electron fluid difficult. One approach to solving the magnetized electron fluid is to utilize a magnetic-field-aligned mesh (MFAM) such as the one in Fig. 1-4.[6] In the MFAM, the boundary of each mesh is precisely aligned with tangential or orthogonal directions of the magnetic lines of force. The use of an MFAM is effective in reducing the numerical diffusion in the computation of magnetized electron fluid. The MFAM-based approach has been a standard approach to calculating the anisotropic magnetized electrons, and MFAM has been used in many research applications such as ion thrusters and tokamak as shown in Fig. 1-5.[17,18] Although the MFAM is effective in computing the magnetized electron fluid, it is not very compatible with the PIC method. The cell sizes in an MFAM typically significantly varies, especially in the magnetic field geometry of plasma lens focusing in Hall thrusters. In general, a minimum number of macro particles of ~ 50 must be maintained in each cell for calculation stability. In the MFAM, this criterion should be satisfied in the cell of minimum sizing. Therefore, if the PIC method is used in the MFAM, one needs to handle quite a number of macro particles in the calculation region, which results in a large computational cost. In terms of the compatibility with PIC methods, a simple mesh whose cell sizes are uniform or varying with plasma density, is preferred.

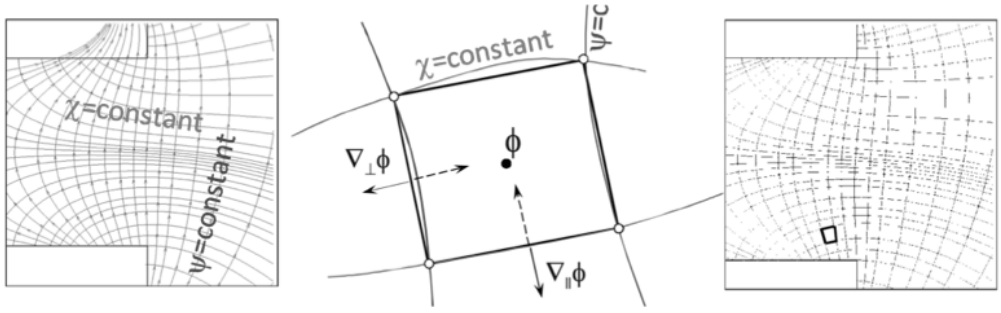

Figure 1-4: The configuration of a two-dimensional magnetic-field-aligned mesh (MFAM).

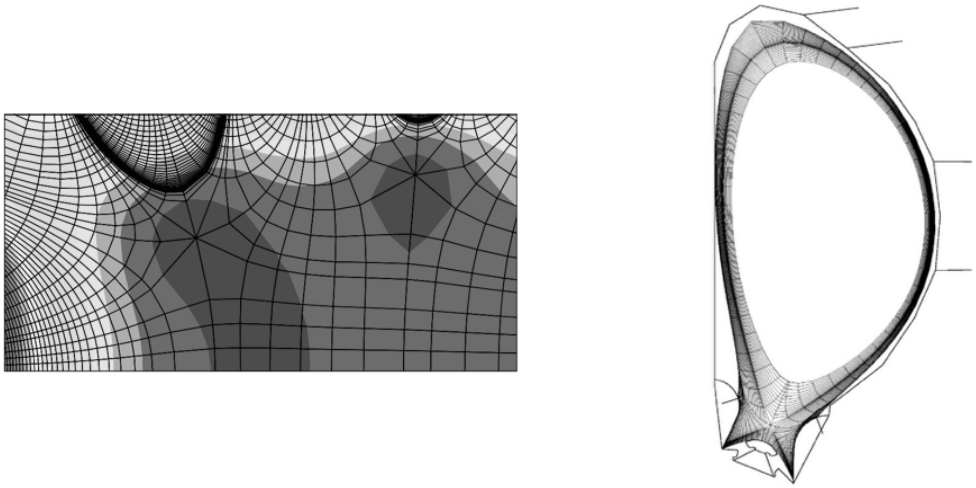

Figure 1-5: (Left): An MFAM used for a calculation of ion thruster. (b): An MFAM used for a tokamak calculation.

Hyperbolic-equation system (HES) approach

In this dissertation, the hyperbolic-equation system (HES) approach for diffusion equations is considered to overcome the difficulties related to magnetized electron fluid.[19–21] Conventionally, diffusion terms are discretized by central differencing because they contribute the stability of computation. Instead, the HES approach solves the diffusion equations by using hyperbolic systems. This approach is supposed to be beneficial in calculating magnetized electron fluid because the approach may avoid the issues associated with anisotropic diffusions.

Herein the mathematical concept of the HES approach is briefly explained. Consider a two-dimensional boundary-value problem for u as follows:

$$-k\nabla^2 u = 0, \tag{1.2}$$

where $k(> 0)$, is a diffusion coefficient. The HES approach divides Eq. (1.2) into hyperbolic equations as follows:

$$\frac{\partial u}{\partial t_{\mathrm{p}}} - k\nabla \cdot \vec{p} = 0, \tag{1.3}$$

$$T_{\mathrm{r}}\frac{\partial p}{\partial t_{\mathrm{p}}} - \nabla u = -\vec{p}, \tag{1.4}$$

where $\vec{p}$ is new variables that approach the gradient of u. t_{p} and T_{r} are pseudo time and arbitrary relaxation time, respectively. To make the pseudo-time advancement terms negligible, the calculation is continued until the steady state is attained. In the steady state, the HES of Eqs. (1.3) and (1.4) is equivalent to Eq. (1.2). Because of the nature of diffusion, the hyperbolic system has two eigenvalues of the same norm and different signs, in each direction, as follows:

$$\lambda_x = -\sqrt{\frac{k}{T_{\mathrm{r}}}},\ \sqrt{\frac{k}{T_{\mathrm{r}}}}, \qquad \lambda_y = -\sqrt{\frac{k}{T_{\mathrm{r}}}},\ \sqrt{\frac{k}{T_{\mathrm{r}}}}. \tag{1.5}$$

A similar concept is also used in the pseudo-compressibility method for low Mach number flows.[22]

Other approaches in mathematics field

Among the computational methods for elliptic equations, a few approaches proposed in the field of mathematics are reviewed. First, the idea of disintegrating a second-order differential equation into several first-order equations is utilized in the mixed finite volume method and mixed finite element method.[23,24] However, in these methods, pseudo-time advancement terms are not introduced, and the system is not recognized as hyperbolic system. Compared with the mixed-type approaches, the HES approach has features that it introduces pseudo-time advancement terms and considers the characteristics of the system in the manner of CFD.

A similar idea to "upwind" is also utilized in the elliptic equation approaches. In the finite volume methods for elliptic equations, one can consider the diffusion flux flowing through cell interfaces. Lipnikov used the concept of right- and left-running waves of information such as the one used in the flux-vector splitting in the evaluation of the diffusion fluxes.[25] Compared with this work, the HES approach has characteristics in its upwind method which is based on the characteristics of the system consisting of multiple equations.

1.6 Objectives and overview of dissertation

There exists a demand of efficient and accurate computational method for magnetized electron fluids which satisfies the conservation laws in two dimensions. Numerical simulations of Hall thruster discharges require such a computational method for analyzing the complicated magnetic field configurations.

The objective of this thesis is to develop a "good" computational method for two-dimensional magnetized electron fluids, in terms of the properties as follows:

1. Efficiency: the computation is fast.
2. Accuracy: the computation yields accurate and reasonable results.
3. Applicability: the computation is applicable to practical problems.

In order to develop such a computational method for magnetized electron fluids, the key idea is the Nishikawa's HES approach. To the best knowledge of the author, Nishikawa mentioned only HES for isotropic diffusion equations. The objective of this thesis is the development of the HES approach which copes with the issues associated with the strong anisotropy of magnetized electron fluids. This thesis proposes an HES for magnetized electron fluid, and develops a computational method which achieves the properties listed above by using several CFD techniques.

This thesis consists of mainly four parts. First, the fundamental equations of magnetized electron fluids are derived in Chapter 2.

In Chapter 3, a hyperbolic-equation system (HES) approach is proposed for magnetized electron fluids. By introducing new variables including the gradient of another variable, the HES of conservation laws is constructed. The HES is stably calculated by an upwind method. The property "1. Efficiency" is discussed via a test calculation by comparing the time to convergence with that of an MFAM-based approach.

In Chapter 4, the HES approach is extended to include the conservation equations of mass, momentum, and energy. To construct an upwind method for the extended HES, a flux-splitting method is proposed. In this method, the fluxes are split into four categories, and the upwind directions of each category is considered. The property "2. Accuracy" is discussed through a test calculation by comparing the mesh convergence

of electron and electron heat flux with those calculated by an MFAM-based approach.

In Chapter 5, the HES approach is applied to the electron fluid calculation in a hybrid modeling of the SPT-100 Hall thruster, to check the property "3. Applicability." The satisfaction level of the Bohm criterion for the wall sheathes is checked, to discuss how accurately the boundary conditions in the electron fluid calculation are reflected to the plasma dynamics.

The conclusions obtained in this thesis are summarized in Chapter 6.

Chapter 2

Fundamental equations of electron fluids

In this chapter, the fundamental equations of electron fluid in quasi-neutral plasmas are derived. Starting from the Boltzmann equation, the conservation equations of magnetized electron fluids are derived. In the derivation process, the two important assumptions: fluid approximation and plasma approximation, are explained.

2.1 Boltzmann equation

In plasmas the motion of a single particle is described by the equation of motion as follows:

$$\frac{\partial \vec{r}}{\partial t} = \vec{v}, \tag{2.1}$$

$$m\frac{\partial \vec{v}}{\partial t} = q\left(\vec{E} + \vec{v} \times \vec{B}\right), \tag{2.2}$$

where m, $\vec{E}$, $\vec{B}$, $\vec{r}$, and $\vec{v}$ are particle mass, electric field, magnetic flux density, position, and velocity, respectively. The collective behavior of particles can be described in a continuum approach. The Boltzmann equation treats the velocity distribution function (VDF) $f(\vec{r}, \vec{v}, t)$ to describe the collective motions. The Boltzmann equation

is described as follows:

$$\frac{\partial f}{\partial t} + \vec{v} \cdot \nabla f + \frac{\vec{F}}{m} \cdot \frac{\partial f}{\partial \vec{v}} = \left(\frac{\partial f}{\partial t} \right)_c . \tag{2.3}$$

Here $\vec{F}$ is outer force acting on the particles and $\left(\frac{\partial f}{\partial t}\right)_c$ represents the collisional effects. In ordinary plasmas, the electromagnetic force is predominant for the outer force. Thus, by using the electromagnetic force for the outer force, the collisional Boltzmann-Vlasov equation is obtained as follows:

$$\frac{\partial f}{\partial t} + \vec{v} \cdot \nabla f + \frac{q}{m} \left(\vec{E} + \vec{v} \times \vec{B} \right) \cdot \frac{\partial f}{\partial \vec{v}} = \left(\frac{\partial f}{\partial t} \right)_c , \tag{2.4}$$

where q is the charge of fluid species. The sign of q is plus for positive ions, and minus for electrons.

2.2 Derivation of conservation equations of fluid

The conservation laws of fluid can be obtained by using moments of the Boltzmann equation. The zeroth-order moment is derived by integrating Eq. (2.4) in the velocity space. The integration yields the mass conservation equation as follows:

$$\frac{\partial n}{\partial t} + \nabla \cdot (n\vec{u}) = \int \left(\frac{\partial f}{\partial t} \right)_c d\vec{v}, \tag{2.5}$$

where n and $\vec{u}$ are number density and average fluid velocity, respectively. The relationship between $\vec{v}$ and $\vec{u}$ is described as follows:

$$\vec{v} = \vec{u} + \vec{w}, \tag{2.6}$$

where $\vec{w}$ is the random thermal velocity. The first-order moment is derived by multiplying Eq (2.4) by $m\vec{v}$ and integrating over the velocity space. This process produces

the momentum conservation equation as follows:

$$mn\frac{\partial \vec{u}}{\partial t} + mn\left(\vec{u}\cdot\nabla\right)\vec{u} + \nabla\cdot[P] - qn\left(\vec{E} + \vec{u}\times\vec{B}\right) = \int m\vec{v}\left(\frac{\partial f}{\partial t}\right)_c d\vec{v}. \tag{2.7}$$

Here $[P]$ is the pressure tensor.

Lastly, the third-order moment is derived by multiplying Eq. (2.4) by $\frac{1}{2}m|\vec{v}|^2$ and integrating over the velocity space. The energy conservation equation is obtained as follows:

$$\frac{\partial U}{\partial t} + \nabla\cdot\left(U\vec{u} + p\vec{u} + \vec{q}_{\rm c}\right) - qn\vec{E}\cdot\vec{u} = \int \frac{1}{2}m|\vec{v}|^2\left(\frac{\partial f}{\partial t}\right)_c d\vec{v}, \tag{2.8}$$

where U is the total energy density which consists of internal and kinetic energies. The second term on left-hand side represents the energy flux including energy convection, work by pressure, and thermal conduction. The third term on left-hand side expresses the Joule heating. With moderate temperature gradient, the thermal conduction flux is approximated by the Fourier's law as follows:

$$\vec{q}_{\rm c} = -\left[\kappa\right]\nabla T, \tag{2.9}$$

where T and $[\kappa]$ are temperature and thermal conductivity tensor. This tensor becomes anisotropic under the presence of magnetic confinement. The collisional term may include the effects of energy dissipation by ionization and excitation collisions.

2.3 Fluid approximation

By implementing the fluid approximation, the information of each particle are averaged and only averaged quantities such as n, $\vec{u}$, and T are treated. This approximation significantly simplifies the numerical simulation in many cases. The fluid approximation is theoretically validated by comparing the representative length of the calculation target, with the characteristic length of the plasma flow featuring the particle effects. If the representative length is much greater than the characteristic length featuring the particle effects, the particle effects may be neglected and the fluid

approximation becomes valid. This section considers two criteria which are commonly used for evaluating the validity of the fluid model.

Knudsen number

In collisional plasmas, the Knudsen number is commonly used for the theoretical validation of fluid approximation. The Knudsen number Kn is expressed as follows:

$$Kn = \frac{\lambda_{\mathrm{m}}}{L}, \tag{2.10}$$

where λ_{m} and L are the mean free path and representative length, respectively. The essential meaning of this number is how many times the particles experience collisions while they traverse the domain where the physical processes happen. It is said that the fluid model may be valid if $Kn < 0.01$. This relation is visualized in Fig. 2-1. In most artificial plasma devices utilizing collisional ionizations, the neutral number density is maintained sufficient for frequent electron-neutral ionization collisions. In this case, the criterion of $Kn < 0.01$ is satisfied for electrons.

Ratio of Larmor radius to scale length

Another aspect on the criterion of fluid approximation is the ratio of Larmor radius as follows:

$$\frac{r_L}{L} = \frac{1}{L}\frac{mv_\perp}{qB}, \tag{2.11}$$

This criterion is used for collisionless plasmas under the presence of magnetic confinement. If $r_L/L < 1$, the fluid model is supposed to be valid.[26] This relation is visualized in Fig. 2-2. In artificial plasma devices, strong magnetic confinements are used to avoid plasma diffusions to the equipment wall. In this case, the condition on the ratio of Larmor radius to scale length of $r_L/L < 1$ is achieved, especially for electrons. Therefore, the fluid equations are valid for electrons in most plasma flows.

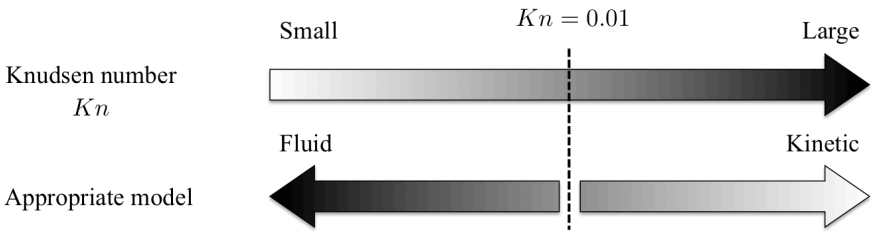

Figure 2-1: The relationship between Knudsen number and appropriate model.

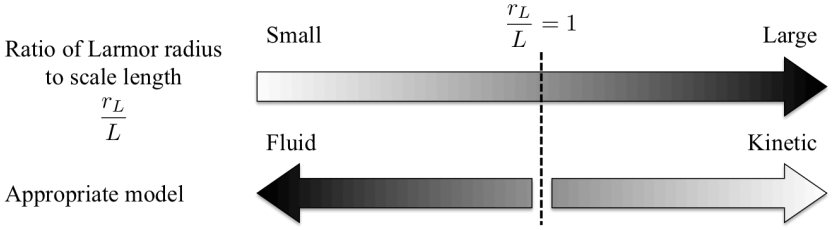

Figure 2-2: The relationship between the ratio of Larmor radius to scale length and appropriate model.

Maxwellian distribution

In the fluid model, the shape of VDF is approximated by the Maxwellian distribution. A VDF of the Maxwellian distribution is described as follows:

$$f_{\mathrm{m}}(v) = \left(\frac{m}{2\pi kT}\right)^{\frac{3}{2}} \exp\left(-\frac{v^2}{v_{\mathrm{th}}^2}\right), \tag{2.12}$$

where

$$v^2 = v_x^2 + v_y^2 + v_z^2, \qquad v_{\mathrm{th}} = \sqrt{\frac{2kT}{m}}. \tag{2.13}$$

A particularly important characteristics of the Maxwellian distribution is the random flux crossing an imaginary plane from one side to the other side. The random flux is formulated as follows:

$$\Gamma_{\mathrm{random}} = \frac{1}{2} n |\bar{v}_x| = \frac{1}{4} |\bar{v}|, \tag{2.14}$$

where

$$|\bar{v}_x| = \sqrt{\frac{2kT}{\pi m}}, \qquad |\bar{v}| = \sqrt{\frac{8kT}{\pi m}}. \tag{2.15}$$

2.4 Quasi-neutrality and plasma approximation

The quasi-neutrality is a reasonable assumption for bulk plasmas in most applications, except for sheaths. One criterion on the validity of quasi-neutrality is the ratio of Debye length λ_{D} to the representative length L. If this ratio λ_{D}/L is sufficiently small, the quasi-neutrality assumption is supposed to be valid. For instance, if $n_{\mathrm{e}} = 10^{18}$ m^{-3}, $T_{\mathrm{e}} = 10$ eV, and $L = 10$ mm are assumed like the condition in Hall thrusters, the Debye length is $\lambda_{\mathrm{D}} = 2.4 \times 10^{-2}$ mm and $\lambda_{\mathrm{D}}/L = 2.4 \times 10^{-3}$. In typical numerical simulations of Hall thrusters, the grid size of $\Delta x/L \sim 10^{-2}$ is sufficient to resolve the phenomena. Therefore, the plasma in each cell is deemed as quasi-neutral.

The assumption of quasi-neutrality does not mean that there is no electric field. It is possible to assume the quasi-neutrality and the existence of electric field at the same time. This process is called as plasma approximation. Chen emphasizes in the book[27] that "*Do not use Poisson's equation to obtain $\vec{E}$ unless it is unavoidale!*" One should exclude the Poisson's equation of Gauss's law, and introduce the new relation of quasi-neutrality. The electric field should be derived through the conservation equations of ions or electrons, if the quasi-neutral assumption is reasonable. Fig. 2-3 graphically summarizes the processes and assumptions to derive the equation set of fluid model with quasi-neutrality. In summary, the electron fluid model with quasi-neutrality is derived by assuming the fluid approximation and quasi-neutrality.

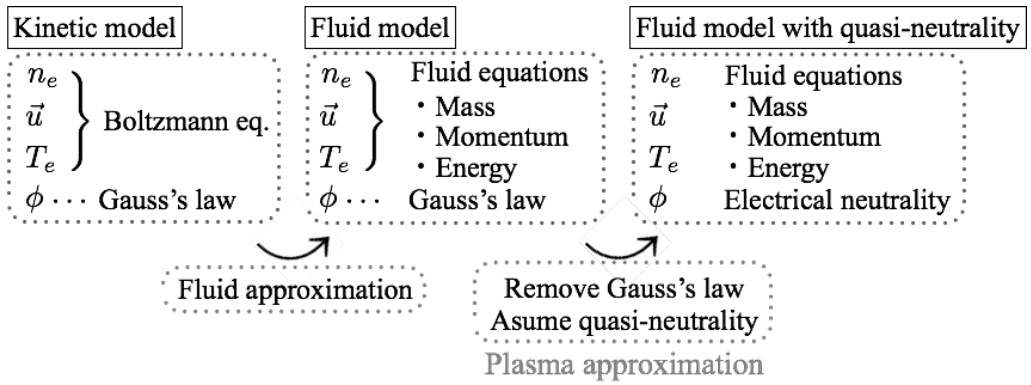

Figure 2-3: Overview of processes and assumptions to derive the equation set of electron fluids quasi-neutral plasmas.

2.5 Conservation equations of electron fluids

The fundamental equations treated herein are the two-dimensional conservation equations of electron mass, momentum, and energy.

Conservation of mass

The mass conservation equation is given by Eq. (2.5). Regarding the collision term on the right-hand side, the effect of ionization is considered. The other effects such as electron attachment and recombination are neglected, because the collision frequency regarding these processes are much smaller than that of the ionization collision in Hall thrusters. Then the conservation of mass is formulated as follows:

$$\frac{\partial n_\mathrm{e}}{\partial t} + \nabla \cdot (n_\mathrm{e} \vec{u}_\mathrm{e}) = n_\mathrm{e} \nu_\mathrm{ion}, \tag{2.16}$$

where n_e, $\vec{u}_\mathrm{e}$, and ν_ion are the electron number density, electron velocity, and ionization collision frequency, respectively. Under the quasi-neutrality assumption, the electron number density is equal to the ion number density. The ion number density is derived through the computation of the ion flow, which is not treated here. Thus, the electron number density can be treated as a given distribution in this thesis. Since electrons are sufficiently mobile to instantaneously achieve quasi-neutrality, the time-derivative term of the electron number density can be excluded. Eq. (2.16) is rewritten as,

$$\nabla \cdot (n_\mathrm{e} \vec{u}_\mathrm{e}) = n_\mathrm{e} \nu_\mathrm{ion}. \tag{2.17}$$

Because the electron density is given as a time-invariant quantity, the electron fluids in quasi-neutral plasmas have characteristics similar to those of incompressible fluids.

Conservation of momentum

The mass conservation equation is originally given by Eq. (2.7). Conservation of momentum is derived from the Navier-Stokes equation,

$$m_\mathrm{e} n_\mathrm{e} \frac{D\vec{u}_\mathrm{e}}{Dt} + \nabla (e n_\mathrm{e} T_\mathrm{e}) - e n_\mathrm{e} \nabla \phi + e n_\mathrm{e} \vec{u}_\mathrm{e} \times \vec{B} = -m_\mathrm{e} n_\mathrm{e} \nu_\mathrm{col} \vec{u}_\mathrm{e}, \tag{2.18}$$

where e, T_e, ϕ, and ν_col are the elemental charge, electron temperature, space potential, and electron-neutral total collision frequency, respectively. The forces working on the fluid element are pressure, electrostatic force, electromagnetic force, and collisional force from the electron-neutral collisions. Here, the effects of electron-electron collision and electron-ion collision are neglected because generally their collision frequencies are much lower than the electron-neutral collision frequency. Furthermore, because of the large number of collisions, the inertia of the electron fluid is negligibly small, and the force working on the fluid element is balanced, so

$$\nabla \left(e n_\mathrm{e} T_\mathrm{e} \right) - e n_\mathrm{e} \nabla \phi + e n_\mathrm{e} \vec{u}_\mathrm{e} \times \vec{B} = -m_\mathrm{e} n_\mathrm{e} \nu_\mathrm{col} \vec{u}_\mathrm{e}. \tag{2.19}$$

After linear conversion of Eq. (2.19), the electron flux in tangential ($||$) and orthogonal ($\perp$) directions of the magnetic lines of force can be described by using the electron mobility μ, as follows:

$$n_\mathrm{e} \begin{pmatrix} u_{||} \\ u_\perp \end{pmatrix} = n_\mathrm{e} \left[\mu\right]_\mathrm{mag} \begin{pmatrix} \nabla_{||} \phi \\ \nabla_\perp \phi \end{pmatrix} - \left[\mu\right]_\mathrm{mag} \begin{pmatrix} \nabla_{||} \left(n_\mathrm{e} T_\mathrm{e} \right) \\ \nabla_\perp \left(n_\mathrm{e} T_\mathrm{e} \right) \end{pmatrix}, \tag{2.20}$$

where

$$\left[\mu\right]_\mathrm{mag} = \begin{bmatrix} \mu_{||} & \\ & \mu_\perp \end{bmatrix} = \begin{bmatrix} \frac{e}{m_\mathrm{e} \nu_\mathrm{col}} & \\ & \frac{\mu_{||}}{1 + \left(\mu_{||} B \right)^2} \end{bmatrix}. \tag{2.21}$$

Eq. (2.20) is Ohm's law for electron current on a coordinate system fitted to magnetic lines of force. In the derivation of Eq. (2.20), the E $\times$ B drift and the diamagnetic drift are neglected by assuming symmetry in one orthogonal direction with the magnetic lines of force. $\mu_\perp$ in Eq. (2.21) is based on the classical diffusion model, and this model can be modified for better reflection of magnetic confinements such as the Bohm diffusion model, depending on the situation.[28] The electron mobility on a computational mesh is derived by rotating $\left[\mu\right]_\mathrm{mag}$ with the angle between the magnetic lines of force and the computational mesh. Thus, we have the following equations.

$$n_\mathrm{e} \vec{u}_\mathrm{e} = n_\mathrm{e} \left[\mu\right] \nabla \phi - \left[\mu\right] \nabla \left(n_\mathrm{e} T_\mathrm{e} \right), \tag{2.22}$$

$$[\mu] = \begin{bmatrix} \mu_x & \mu_c \\ \mu_c & \mu_y \end{bmatrix} = \Theta^{-1} [\mu]_{\mathrm{mag}} \Theta, \qquad \Theta = \begin{bmatrix} \cos\theta & -\sin\theta \\ \sin\theta & \cos\theta \end{bmatrix}. \tag{2.23}$$

Here Θ is the rotation matrix and θ is the angle between the magnetic lines of force and the computational mesh.

Conservation of energy

When considering the energy conservation equation of Eq. (2.8) for electrons, the internal energy is predominant since the electron mass is quite small. In addition to this, electrons can be treated as monoatomic molecule, thus $U = \frac{3}{2} e n_e T_e$. Then, the equation of energy conservation is formulated as follows:

$$\frac{\partial}{\partial t}\left(\frac{3}{2} e n_e T_e\right) + \nabla \cdot \left(\frac{5}{2} e n_e T_e \vec{u}_e - [\kappa] \nabla T_e\right) = e n_e \vec{u}_e \cdot \nabla \phi - \alpha e \varepsilon_{\mathrm{ion}} n_e \nu_{\mathrm{ion}}. \tag{2.24}$$

where $\varepsilon_{\mathrm{ion}}$ is the single ionization energy. Here α is a coefficient to handle the effects of ionization, excitation, and radiation with a single term, and it is experimentally determined as a function of electron temperature.[29] For instance, this function is expressed for xenon as follows:

$$\alpha = 2.0 + 0.254 \exp\left(0.667 \frac{\varepsilon_{\mathrm{ion}}}{T_e}\right). \tag{2.25}$$

The relation between the thermal conductivity and thermal diffusivity is formulated as follows:

$$[\kappa] = n_e c_p [D_t], \tag{2.26}$$

where D_t is the thermal diffusivity. The process of thermal diffusion is associated with electron diffusion, thus,

$$[D_t] \simeq [D_e], \tag{2.27}$$

where D_e is the diffusion coefficient of electrons. By using the Einstein relation of $[D_e] = T_e [\mu]$,[30] the thermal conductivity is eventually expressed as follows:

$$[\kappa] = n_e c_p [D_e] = \frac{5}{2} e n_e T_e [\mu]. \tag{2.28}$$

Chapter 3

A hyperbolic-equation system approach for electron fluids

In this chapter, a new approach using a hyperbolic-equation system (HES) is proposed to solve for the anisotropic diffusion equation of magnetized electron fluids in quasi-neutral plasmas. The conventional approach using an elliptic equation suffers numerical instabilities stemming from the cross diffusion terms. The HES approach avoids treatments of cross-diffusion terms. The HES is constructed by introducing new variables which contain gradient of another variable. A test calculation reveals that the HES approach can robustly solve problems of strong magnetic confinement by using an upwind method. The computation time of the HES approach is compared with that of the MFAM-based EE approach in terms of the size of the problem and the strength of magnetic confinement. The results indicate that the HES approach can be used to solve problems in a simple structured mesh without increasing computational time compared to the MFAM-based EE approach and that it features fast convergence in conditions of strong magnetic confinement.

3.1 Issues of conventional approaches using an elliptic equation

A common approach to computing the space potential is to utilize an integrated form of the mass conservation equation and momentum conservation equations.[31,32] Substituting the divergence of Eq. (2.22) into Eq. (2.17) gives an elliptic equation as follows:

$$\nabla \cdot \left(n_{\mathrm{e}} \left[\mu \right] \nabla \phi - \left[\mu \right] \nabla \left(n_{\mathrm{e}} T_{\mathrm{e}} \right) \right) = n_{\mathrm{e}} \nu_{\mathrm{ion}}. \tag{3.1}$$

This equation is solved for the space potential as a boundary value problem. This approach is similar to the marker-and-cell (MAC) approach for incompressible fluids in the sense that both utilize an elliptic equation derived by the divergence of the momentum conservation equation.[33] The approach using Eq. (3.1) is referred to as the EE approach in this paper.

The first term on the left-hand side of Eq. (3.1) can be decomposed as follows:

$$\nabla \cdot \left(n_{\mathrm{e}} \begin{bmatrix} \mu_{\mathrm{x}} & \mu_{\mathrm{c}} \\ \mu_{\mathrm{c}} & \mu_{\mathrm{y}} \end{bmatrix} \nabla \phi \right) = \frac{\partial}{\partial x} \left(n_{\mathrm{e}} \mu_{\mathrm{x}} \frac{\partial \phi}{\partial x} \right) + \frac{\partial}{\partial y} \left(n_{\mathrm{e}} \mu_{\mathrm{y}} \frac{\partial \phi}{\partial y} \right) + \frac{\partial}{\partial x} \left(n_{\mathrm{e}} \mu_{\mathrm{c}} \frac{\partial \phi}{\partial y} \right) + \frac{\partial}{\partial y} \left(n_{\mathrm{e}} \mu_{\mathrm{c}} \frac{\partial \phi}{\partial x} \right) \tag{3.2}$$

In Eq. (3.2), μ_{x} and μ_{y} are coefficients for diffusion terms of $\partial^2/\partial x^2$ and $\partial^2/\partial y^2$, and μ_{c} is the coefficient for the cross-diffusion terms of $\partial^2/\partial x \partial y$. Both these two types of diffusion terms pose difficulties if Eq. (3.1) is solved with an iterative method. The first difficulty is due to the large difference between μ_{x} and μ_{y}, which increases the condition number of the problem and degrades convergence performance.

The more critical difficulty is that the cross-diffusion terms violate the diagonal dominance of the coefficient matrix. The condition of diagonal dominance is formulated as follows if elements in coefficients matrix is expressed as a.

$$|a_{ii}| \geq \sum_{j \neq i} |a_{ij}| \qquad for\ all\ i \tag{3.3}$$

Here the index i is for rows, and the index j is for columns. To satisfy this criterion, it is important to maintain the balence between diagonal and nondiagonal elements in discretization. The contribution of the coefficient in stencils to diagonal and nondiagonal elements of the coefficient matrix in one row is shown in Fig. 3-1 for convection, diffusion, and cross-diffusion terms. Convection and diffusion terms increase both the diagonal and nondiagonal elements by the same value, and diagonal dominance is maintained. However, in differencing cross-diffusion terms, the increase of nondiagonal elements is greater than that of diagonal elements with any discretization method based on linear Taylor expansions. The violation of diagonal dominance of the coefficient matrix constrains the convergence speed by $\mu_c/\Delta x \Delta y$. This restriction is very severe in many cases, which results in quite slow convergence. Although one can use a direct method to compute Eq. (3.1), the computation cost is $O\left(N_{\text{cell}}^3\right)$, where N_{cell} is the number of cells. Thus, using a direct method is not desired for practical simulations.

Because the cross-diffusion terms are caused by the angle between the computational mesh and the magnetic lines of force, one effective approach to avoid cross-diffusion terms is to use an magnetic-field-aligned mesh (MFAM).[6] By aligning the computational mesh with the magnetic lines of force precisely, the effect of cross diffusion is neglected. If only non-cross-diffusion terms are included in Eq. (3.1), the diagonal dominance of the coefficient matrix is satisfied by applying a central difference to the diffusion terms. However, if the magnetic lines of force near the boundary are neither parallel nor perpendicular to the boundary, the MFAM ceases to be a body-fitted mesh and the estimation of fluxes flowing into the boundary becomes complicated. Also, if the magnetic field is time variant such as the induced magnetic field, the mesh needs to be reconstructed in every iteration, which results in large computation costs. Using a MFAM is effective in avoiding cross-diffusion terms but its application range is limited.

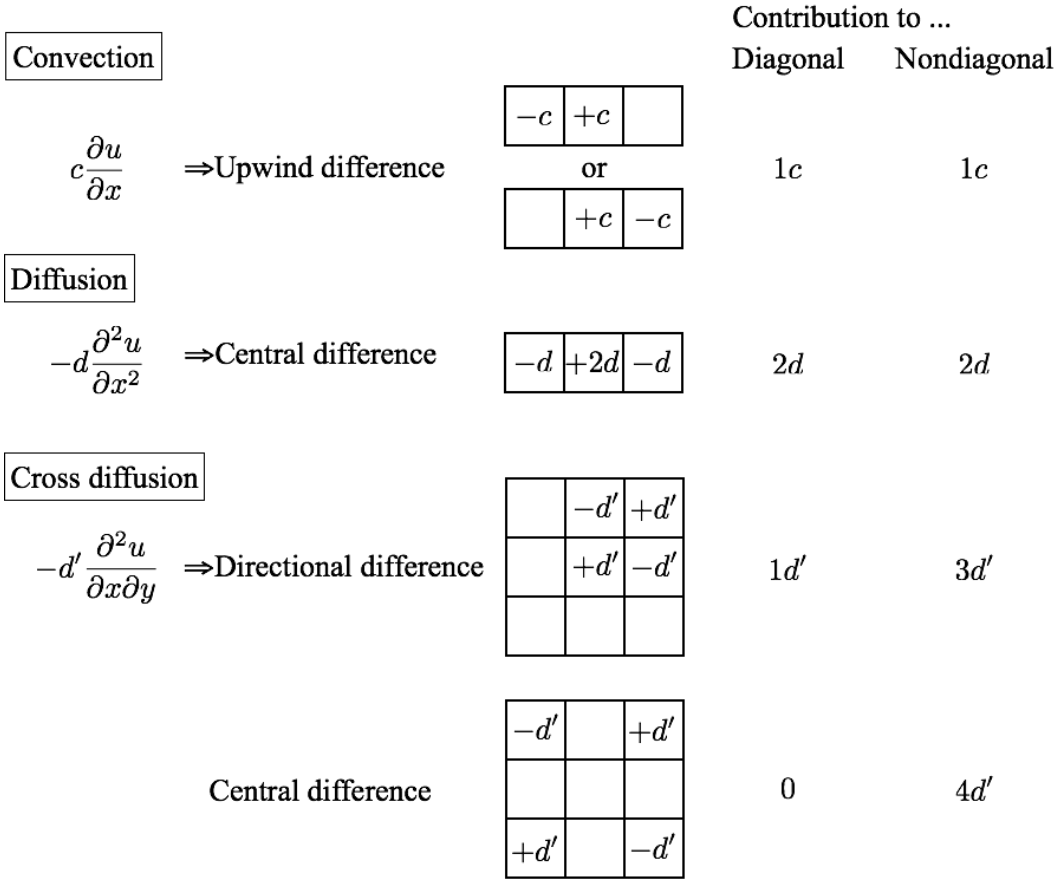

Figure 3-1: Contribution of coefficients in stencils of convection, diffusion, and cross-diffusion terms to diagonal and nondiagonal elements of the coefficient matrix. The balance of diagonal and nondiagonal terms is violated in differencing cross-diffusion terms.

3.2 The hyperbolic-equation system approach

3.2.1 Construction of a hyperbolic-equation system

Another approach to avoid cross-diffusion terms is the hyperbolic-equation system (HES) approach. In this approach one converts the second-order differential equation into a first-order system by introducing new variables, which include the gradient of another variable. This kind of approach was first proposed by Nishikawa for future application to Navier-Stokes equations.[19,20] Nishikawa mentioned following remarks about the HES approach in his papers.[19,20]

- Diffusion equations and advection-diffusion equations can be solved with upwind

schemes.

- Both of advection and diffusion terms can be solved by a single advection scheme.
- The gradient of variables can be calculated in the same order of accuracy as main variables.
- High-order accuracy schemes are applicable as well as common advection equations.

Although Nishikawa did not mention cross-diffusion terms in his papers, the HES approach is supposed to be beneficial in solving anisotropic diffusion equations including cross-diffusion terms.

Instead of the elliptic equation of Eq. (3.1), the original mass and momentum conservation equations can be used for an HES. To solve for the space potential in an HES, a pseudo-time advancement term of the space potential is introduced into Eq. (2.17). Also, pseudo-time advancement terms of electron momentum are added to Eq. (2.22) for x- and y-directions. Then the HES of electron fluids in quasi-neutral plasmas can be derived as follows:

$$\frac{1}{a}\frac{n_\mathrm{e}}{T_\mathrm{e}}\frac{\partial \phi}{\partial t} - \nabla \cdot (n_\mathrm{e}\vec{u}_\mathrm{e}) = -n_\mathrm{e}\nu_\mathrm{ion}, \tag{3.4}$$

$$\frac{1}{\nu_\mathrm{col}} \begin{bmatrix} b_\mathrm{x} & \\ & b_\mathrm{y} \end{bmatrix}^{-1} \frac{\partial}{\partial t}(n_\mathrm{e}\vec{u}_\mathrm{e}) - n_\mathrm{e}[\mu]\nabla\phi + [\mu]\nabla(n_\mathrm{e}T_\mathrm{e}) = -n_\mathrm{e}\vec{u}_\mathrm{e}, \tag{3.5}$$

where a, b_x, and b_y are arbitrary acceleration parameters of no dimension. Because the pseudo-time advancement terms are artificially added, the HES of Eqs. (3.4) and (3.5) needs to be calculated until a steady state is obtained to make the artificial terms negligibly small. In a steady state, the HES is equivalent to the mass and momentum conservation equations. This approach is similar to the pseudo-compressibility approach for incompressible fluids in the sense that both introduce a pseudo-time advancement term into the conservation equation.[22] However, the key point of this

approach is to add the pseudo-time advancement term of the space potential in the mass conservation equation, but not that of electron density. The introduction of the pseudo-time advancement term of space potential is discusses in Sec. 3.7 in detail.

3.2.2 Nondimensional form of the hyperbolic-equation system

Eqs. (3.4) and (3.5) are modified to a nondimensional form for the analysis. First, the electron mobility tensor is normalized by the electron mobility in the tangential direction of the magnetic lines of force:

$$[\tilde{\mu}] = \begin{bmatrix} \tilde{\mu}_{\mathrm{x}} & \tilde{\mu}_{\mathrm{c}} \\ \tilde{\mu}_{\mathrm{c}} & \tilde{\mu}_{\mathrm{y}} \end{bmatrix} = \frac{1}{\mu_{\parallel}} [\mu] = \frac{m_{\mathrm{e}}\nu_{\mathrm{col}}}{e} [\mu] . \tag{3.6}$$

By using representative values of electron number density n_{e}^*, electron temperature T_{e}^* and mean free path λ_{m}^*, the nondimensional values of the physical quantities are defined as follows:

$$\tilde{n}_{\mathrm{e}} = \frac{n_{\mathrm{e}}}{n_{\mathrm{e}}^*}, \qquad \tilde{T}_{\mathrm{e}} = \frac{T_{\mathrm{e}}}{T_{\mathrm{e}}^*}, \qquad \tilde{\phi} = \frac{\phi}{T_{\mathrm{e}}^*}, \qquad (\tilde{x}, \tilde{y})^T = \frac{1}{\lambda_{\mathrm{m}}^*} (x, y)^T , \tag{3.7}$$

$$\tilde{t} = \frac{1}{\tau_{\mathrm{m}}^*} t = \frac{v_{\mathrm{e,th}}^*}{\lambda_{\mathrm{m}}^*} t = \frac{1}{\lambda_{\mathrm{m}}^*} \sqrt{\frac{2eT_{\mathrm{e}}^*}{m_{\mathrm{e}}}} t, \qquad \tilde{\vec{u}}_{\mathrm{e}} = \frac{\vec{u}_{\mathrm{e}}}{c_{\mathrm{s}}^*} = \frac{\vec{u}_{\mathrm{e}}}{\sqrt{\frac{\gamma eT_{\mathrm{e}}^*}{m_{\mathrm{e}}}}}, \tag{3.8}$$

$$\tilde{\nu}_{\mathrm{col}} = \tau_{\mathrm{m}}^* \nu_{\mathrm{col}}, \qquad \tilde{\nu}_{\mathrm{ion}} = \tau_{\mathrm{m}}^* \nu_{\mathrm{ion}}. \tag{3.9}$$

Here the tilde denotes a nondimensional quantity. τ_{m}, $v_{\mathrm{e,th}}$, and c_{s} are the mean free time, electron thermal velocity, and electron acoustic velocity, respectively. By using these quantities, a nondimensional equation system can be constructed. Furthermore, the following properties are assumed throughout the calculation region for simplified analysis of the space potential and electron velocity.

$$\tilde{n}_{\mathrm{e}} = 1, \qquad \tilde{T}_{\mathrm{e}} = 1, \qquad \tilde{\nu}_{\mathrm{col}} = 1, \qquad \tilde{\nu}_{\mathrm{ion}} = 0. \tag{3.10}$$

Eventually, the simplified nondimensional system can be expressed as follows:

$$\frac{1}{a}\frac{\partial\tilde{\phi}}{\partial\tilde{t}} - \sqrt{\frac{\gamma}{2}}\tilde{\nabla}\cdot\vec{\tilde{u}}_{\mathrm{e}} = 0, \tag{3.11}$$

$$\begin{bmatrix} b_{\mathrm{x}} & \\ & b_{\mathrm{y}} \end{bmatrix}^{-1} \frac{\partial\vec{\tilde{u}}_{\mathrm{e}}}{\partial\tilde{t}} - \frac{1}{\sqrt{2\gamma}}\left[\tilde{\mu}\right]\tilde{\nabla}\tilde{\phi} = -\vec{\tilde{u}}_{\mathrm{e}}. \tag{3.12}$$

Optimal choice of the acceleration parameters improves the condition of the numerical problem. One of the criteria controlling the difficulty of the numerical problem is the condition number. In this problem the condition number can be interpreted as the absolute value of the ratio of the maximum eigenvalue to the minimum eigenvalue in the coefficient matrix. Thus, to make the eigenvalues unity in each direction the acceleration coefficients are chosen as follows:

$$a = \sqrt{\frac{2}{\gamma}}, \qquad b_{\mathrm{x}} = \frac{\sqrt{2\gamma}}{\tilde{\mu}_{\mathrm{x}}}, \qquad b_{\mathrm{y}} = \frac{\sqrt{2\gamma}}{\tilde{\mu}_{\mathrm{y}}}. \tag{3.13}$$

With these acceleration coefficients, Eqs. (3.11) and (3.12) can be rewritten in the vector form as follows:

$$\frac{\partial U}{\partial\tilde{t}} + J_x\frac{\partial U}{\partial\tilde{x}} + J_y\frac{\partial U}{\partial\tilde{y}} = S, \tag{3.14}$$

$$U = \left(\tilde{\phi}, \tilde{u}_{\mathrm{x}}, \tilde{u}_{\mathrm{y}}\right)^T, \qquad S = \left(0, -\frac{\sqrt{2\gamma}}{\tilde{\mu}_{\mathrm{x}}}\tilde{u_{\mathrm{x}}}, -\frac{\sqrt{2\gamma}}{\tilde{\mu}_{\mathrm{y}}}\tilde{u_{\mathrm{y}}}\right)^T \tag{3.15}$$

$$J_x = \begin{pmatrix} 0 & -1 & 0 \\ -1 & 0 & 0 \\ -\frac{\tilde{\mu}_{\mathrm{c}}}{\tilde{\mu}_{\mathrm{y}}} & 0 & 0 \end{pmatrix}, \qquad J_y = \begin{pmatrix} 0 & 0 & -1 \\ -\frac{\tilde{\mu}_{\mathrm{c}}}{\tilde{\mu}_{\mathrm{x}}} & 0 & 0 \\ -1 & 0 & 0 \end{pmatrix}. \tag{3.16}$$

Here, J_x and J_y are the Jacobian matrices in the x and y directions. The eigenvalues for the Jacobian matrices are as simple as follows:

$$\lambda_x = 0, \pm 1, \qquad \lambda_y = 0, \pm 1. \tag{3.17}$$

By using the Jacobian matrices and the eigenvalues, upwind schemes based on the approximate Riemann solver can be constructed.

Here the meaning of the characteristic speeds in Eq. (3.17) is discussed.For instance, the characteristic quantities for the eigenvalues in the x-direction of $\lambda_x = 0, \pm 1$ are $-\frac{\tilde{\mu_c}}{\tilde{\mu_y}}\tilde{u}_x + \tilde{u}_y, \pm\tilde{\phi} + \tilde{u}_x$, respectively. The zero characteristic speed indicates that the information of $-\frac{\tilde{\mu_c}}{\tilde{\mu_y}}\tilde{u}_x + \tilde{u}_y$ is not transported in the x-direction. Likewise, the information of $-\frac{\tilde{\mu_c}}{\tilde{\mu_x}}\tilde{u}_y + \tilde{u}_x$ is not conveyed in the y-direction.

3.3 Test calculation condition and numerical method

3.3.1 Calculation condition in two dimensions

Test calculations in two dimensions are conducted for the analyses of the HES approach for the electron fluid equations. Another intention of the test is to compare the HES and EE approaches in terms of the computation cost. The calculation condition is illustrated in Fig. 3-2-(a). Magnetic lines of force, uniformly angled at 45° from the vertical and with uniform strength of magnetic confinement of $\mu_{||}/\mu_{\perp} = 1000$, are applied on the calculation field. Dirichlet conditions on the nondimensional space potential are defined at the left and right side boundaries. Zero-flux conditions are used for the top and bottom boundaries. The condition of 45° magnetic lines of force gives a maximum effect of cross diffusion in the EE approach when a vertical-horizontal mesh (VHM) is used. Thus if this condition can be solved stably with the HES approach, robust calculations for any angle of magnetic lines of force can be expected.

Also, to confirm that the HES approach is applicable to a condition with complicated configuration of magnetic lines of force, a condition of concave magnetic lines of force is calculated with the HES approach. This calculation condition is illustrated in Fig. 3-2-(b). The magnetic lines of force are angled by -63.5° to 63.5° from the vertical line in the calculation field. The uniform strength of magnetic confinement of $\mu_{||}/\mu_{\perp} = 1000$ is assumed. Nondimensional space potential is defined at the left and right boundaries, and nondimensional electron velocity in y-direction is defined for the top and bottom boundaries.

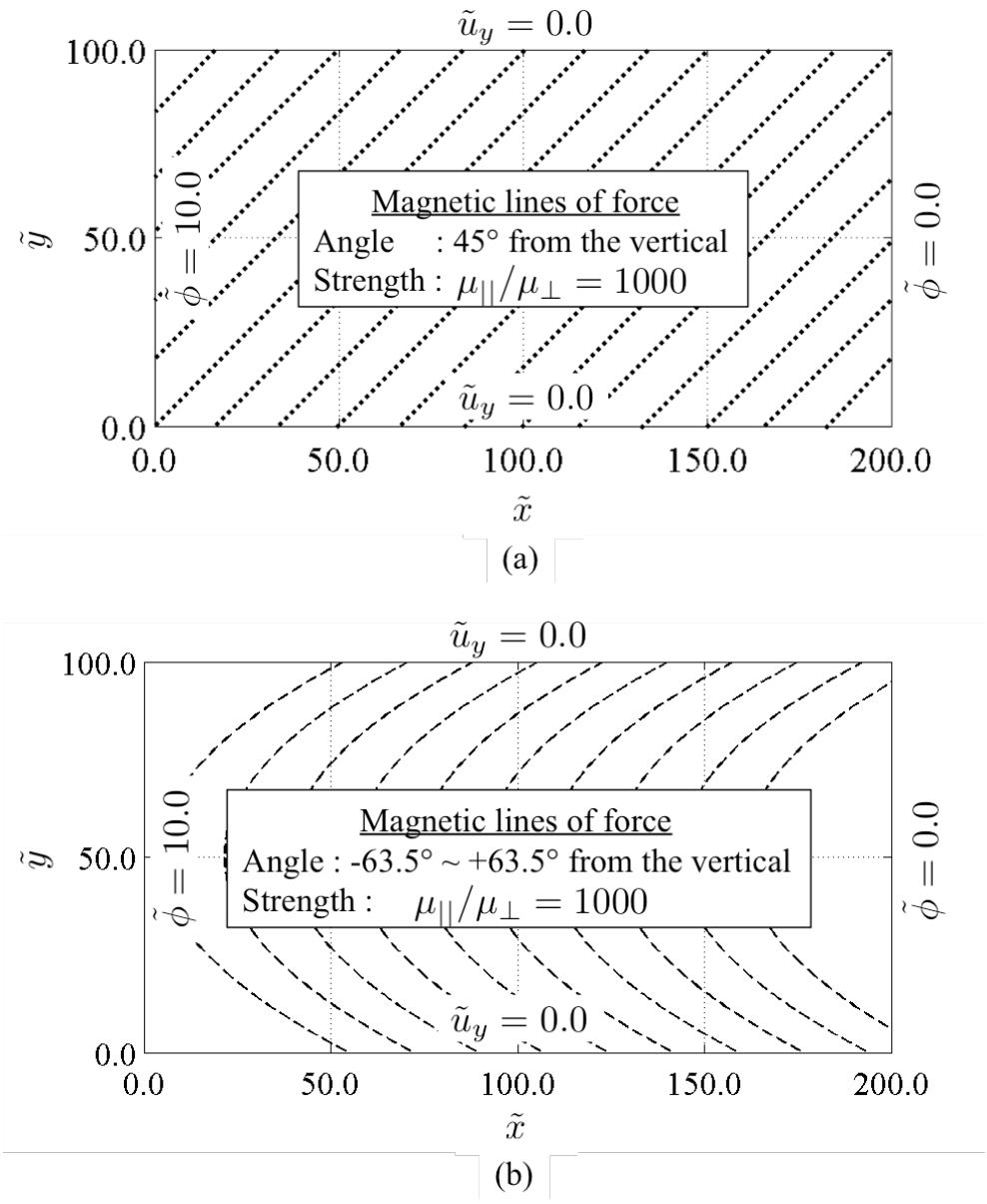

Figure 3-2: Two-dimensional calculation conditions used for the test calculation. (a): The magnetic lines of force are uniformly angled by 45°. (b): A concave shape of magnetic lines of force toward right-hand side are applied with the angle from the vertical of -63.5° at the bottom and 63.5° at the top of the calculation field. For both cases the strength of magnetic confinement of $\mu_{||}/\mu_{\perp} = 1000$ is assumed. Dirichlet conditions are used on $\tilde{\phi}$ for the left and right side boundaries. The zero-flux condition is used for the top and bottom boundaries.

3.3.2 Numerical method used in the HES approach

The numerical methods used for the HES approach are summarized in Table 3.1. The discretization is implemented based on a finite-difference method. A first-order upwind scheme is constructed based on the Jacobian matrices and the eigenvalues of Eqs. (3.16) and (3.17). Here the upwind difference based on an approximate Riemann solver of Steger-Warming's flux vector splitting (FVS) is used.[34] The FVS is modified for the non-conservation form of Eq. (3.14).[35] For instance, the space difference in the $\tilde{x}$ direction is split as follow:

$$J_{\mathrm{x}}\frac{\partial U}{\partial \tilde{x}} \simeq \frac{1}{\Delta\tilde{x}} J_{\mathrm{x}}^{+}\delta_{\mathrm{x}}^{b}U + \frac{1}{\Delta\tilde{x}} J_{\mathrm{x}}^{-}\delta_{\mathrm{x}}^{f}U. \tag{3.18}$$

Here, J_{x}^{+} and J_{x}^{-} are the Jacobian matrices which have only positive and negative eigenvalues, and δ_{x}^{f} and δ_{x}^{b} are the forward and backward derivatives, respectively. Because the signs of the eigenvalues are fixed, the split terms in Eq. (3.18) are always differentiable. Thus the scheme does not lead to instability associated with the change of signs in eigenvalues.

Implicit methods should be used for the pseudo-time advancement method because only the steady-state solution is needed. In an implicit method, the space difference is evaluated at the $n+1$ time level. Eq. (3.14) can be written by discretizing the time-derivative term in the first-order form as:

$$\frac{\Delta U^{n}}{\Delta\tilde{t}} + \left(J_x\frac{\partial U}{\partial\tilde{x}} + J_y\frac{\partial U}{\partial\tilde{y}}\right)^{n+1} = S^{n}, \tag{3.19}$$

where $\Delta\tilde{t}$ is the time step and $\Delta U^{n} = U^{n+1} - U^{n}$. This formulation is converted to a "delta" form of the implicit method by utilizing Beam-Warming linearization.[36]

$$\left(I + \Delta\tilde{t}J_x^{n}\frac{\partial}{\partial\tilde{x}} + \Delta\tilde{t}J_y^{n}\frac{\partial}{\partial\tilde{y}}\right)\Delta U^{n} = -\Delta\tilde{t}\left(J_x\frac{\partial U}{\partial\tilde{x}} + J_y\frac{\partial U}{\partial\tilde{y}}\right)^{n} + \Delta\tilde{t}S^{n}. \tag{3.20}$$

For the two-dimensional calculation, the alternating direction implicit (ADI) method is used for fast computation. In the EE approach, the ADI method cannot be used if there are cross-diffusion terms. Information on the stencils of $(i+1, j+1)$,

Table 3.1: Summary of the HES and EE approaches. VHM: vertical-horizontal mesh. MFAM: magnetic-field-aligned mesh.

	HES approach	EE approach
Equation	Hyperbolic-equation system (HES)	Elliptic equation (EE)
Mesh	VHM	MFAM
Scheme	First-order upwind	Second-order central
Iteration	LU-ADI method	SOR method

$(i-1, j+1)$, $(i+1, j-1)$, or $(i-1, j-1)$ must be used for cross-diffusion terms if the differencing is based on a linear Taylor series in two dimensions. The coefficients for these stencils appear in isolated positions from diagonal positions in the coefficient matrix; thus reduction of computation cost by ADI is not expected. However, in the HES approach, the ADI method can be used because cross-diffusion terms are not included. The ADI factorization proposed by Beam and Warming is applied to Eq. (3.20) as follow:[36]

$$\left(I + \Delta\tilde{t} J_x^n \frac{\partial}{\partial \tilde{x}}\right)\left(I + \Delta\tilde{t} J_y^n \frac{\partial}{\partial \tilde{y}}\right)\Delta U^n = -\Delta\tilde{t}\left(J_x \frac{\partial U}{\partial \tilde{x}} + J_y \frac{\partial U}{\partial \tilde{y}}\right)^n + \Delta\tilde{t} S^n. \quad (3.21)$$

To strengthen the diagonal dominance, an lower-upper ADI (LU-ADI) scheme is further implemented.[37] In the LU-ADI method, for instance, the operator in the $\tilde{x}$ direction can be written as follow:

$$I + \Delta\tilde{t} J_x \frac{\partial}{\partial \tilde{x}} \simeq \left(I - \frac{\Delta\tilde{t}}{\Delta\tilde{x}} J_x^- + \Delta\tilde{t} J_x^+ \delta_x^b\right)\left(I + \frac{\Delta\tilde{t}}{\Delta\tilde{x}}\left(J_x^+ - J_x^-\right)\right)^{-1}\left(I + \frac{\Delta\tilde{t}}{\Delta\tilde{x}} J_x^+ + \Delta\tilde{t} J_x^- \delta_x^f\right). \quad (3.22)$$

The computations are implemented with a Courant number of 30.

For the HES approach, a VHM is used as shown in Fig. 3-3-(a). The boundary conditions are set at the "ghost cells" outside of the calculation field. According to the eigenvalues of Eq. (3.17), one characteristic speed is flowing from outside to inside of the boundary. Thus, among the three variables of Eq. (3.15), one variable should be defined as the boundary condition. The calculation condition of Fig. 3-2 satisfies this requirement on the boundary conditions.

3.3.3 Numerical method used in the EE approach

For the condition in Fig. 3-2, the dimensionless elliptic equation for space potential can be written as follows:

$$\tilde{\nabla}_{\mathrm{m}} \cdot \left([r]_{\mathrm{m}} \tilde{\nabla}_{\mathrm{m}} \tilde{\phi} \right) = 0, \tag{3.23}$$

$$[r]_{\mathrm{m}} = \begin{bmatrix} 1 & \\ & \frac{\tilde{\mu}_{\perp}}{\tilde{\mu}_{||}} \end{bmatrix}, \qquad \tilde{\nabla}_{\mathrm{m}} = \begin{pmatrix} \dfrac{\partial}{\partial \xi} & \dfrac{\partial}{\partial \eta} \end{pmatrix}^{T}, \tag{3.24}$$

where ξ and η mean tangential and orthogonal directions of magnetic lines of force, respectively. The numerical methods used for the EE approach are also summarized in Table 3.1. The EE approach with an MFAM handles only non-cross-diffusion terms. Thus a second-order central difference is used with the finite-volume method. To solve the boundary value problem of the elliptic equation, a successive over-relaxation (SOR) method is used. In the test calculations the relaxation parameter of the SOR is set as 1.8. For the EE approach, an MFAM is used, as is shown in Fig. 3-3 (b). This mesh is derived by rotating the VHM by 45°. The boundary conditions are defined at ghost cells outside the calculation field. For the upper and lower boundary conditions of $u_{\mathrm{y}} = 0$, the electron mass flux is set to zero.

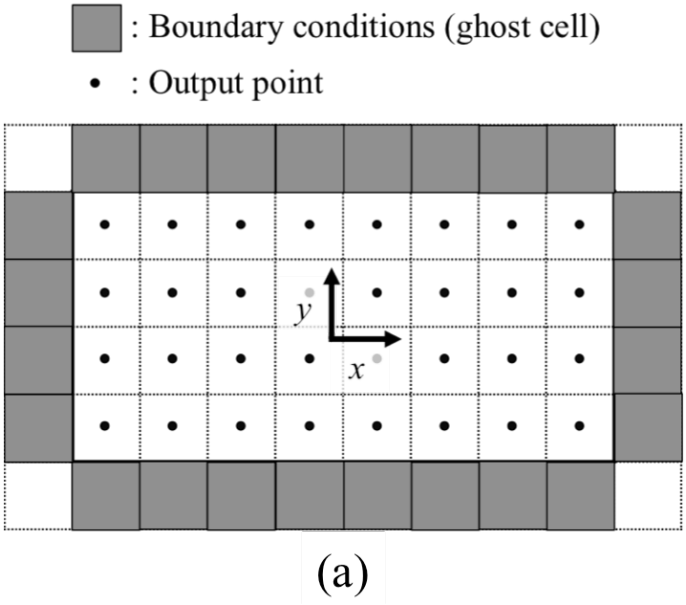

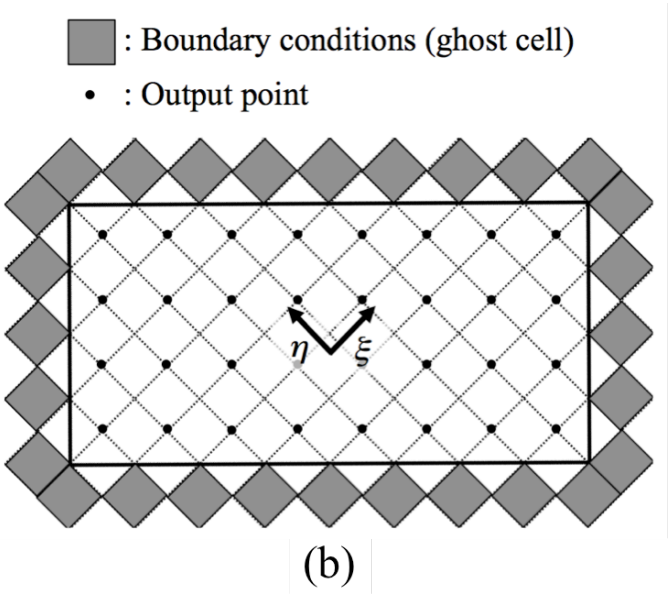

Figure 3-3: (a): A VHM for a grid of 8 × 4 (output points). (b): An MFAM for a grid of 8 × 4 (output points).

3.4 Steady-state calculation results

The HES approach is tested for the calculation condition of Fig. 3-2-(a) with a VHM for a grid of 48 × 24. The steady-state calculation results are shown in Fig. 3-4. The equipotential lines are almost uniformly angled by 45°, which indicates that the result reflects the effect of magnetic confinement. Also, the velocity vector map reflects the zero-flux boundary condition at the top and bottom boundaries. Because the HES approach utilizes pseudo-time advancement terms, they have to converge to be negligibly small values in the steady state. For evaluating the convergence of each variable, the normalized difference is defined as

$$D_{\mathrm{norm}} = \sqrt{\frac{1}{N_{\mathrm{cell}}} \sum^{N_{\mathrm{cell}}} \left(\frac{|y^{n+1} - y^n|^2}{|y^n|^2 + \varepsilon} \right)}. \tag{3.25}$$

Here y is a variable and ε is a positive value satisfying $\varepsilon \ll |y|$ to avoid division by zero. The time history of the normalized difference of each variable is shown in Fig. 3-5. The normalized difference of each variable shows a monotone decrease, and they become negligibly small in the steady state. This fact verifies the usefulness of pseudo-time advancement terms and that a robust calculation is possible with the HES approach for the conditions of angled magnetic lines of force.

The condition of Fig. 3-2 (b) is also calculated by the HES approach using a VHM for a grid of 48 × 24. The steady-state calculation results and the time history of the normalized difference are shown in Fig. 3-6 and Fig. 3-7, respectively. It is confirmed that the equipotential lines reflect the magnetic lines of force and all of the pseudo-time advancement terms become negligibly small values in the steady state. This indicates that the HES approach can robustly compute the condition of complicated magnetic lines of force configuration.

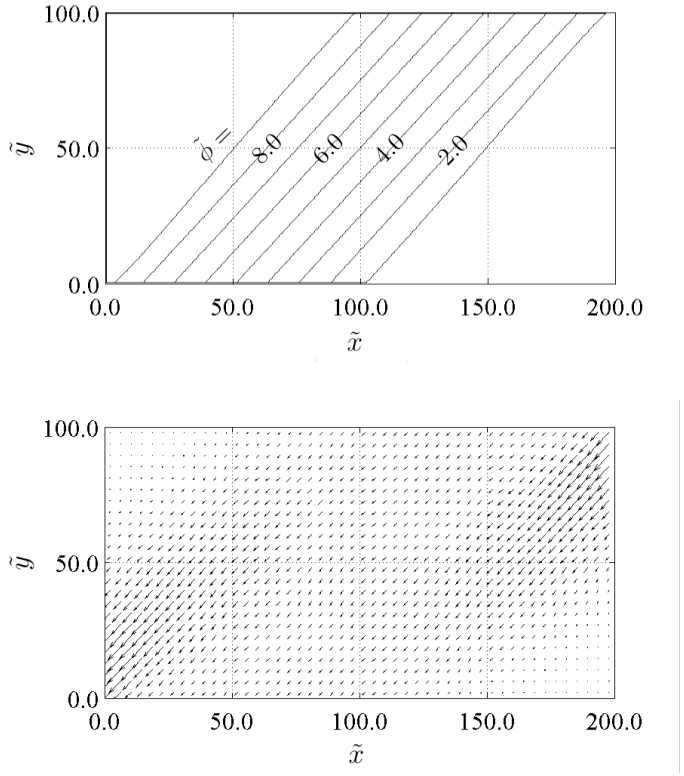

Figure 3-4: Simulation results for the Fig. 3-2 (a) condition with the HES approach using a VHM grid of 48 × 24. Top: Nondimensional space potential distribution. Bottom: Vector map of nondimensional velocity.

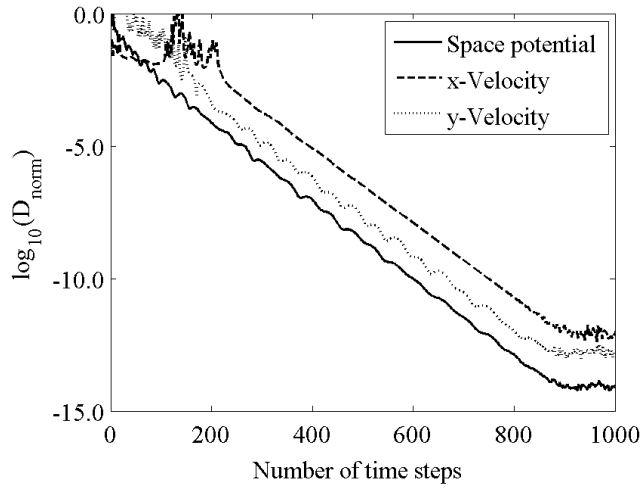

Figure 3-5: Time history of the normalized difference of each variable. The Fig. 3-2 (a) condition is solved with the HES approach using a 48 × 24 grid.

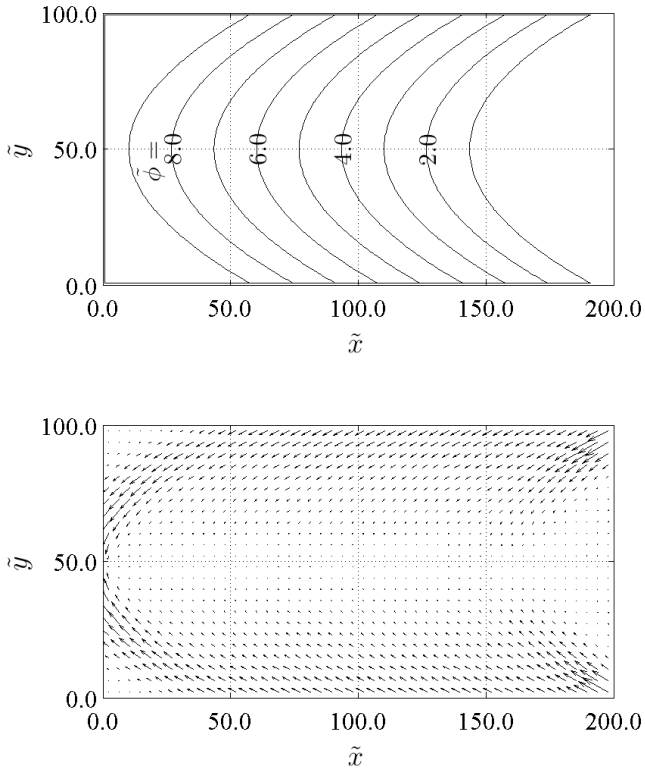

Figure 3-6: Simulation results for the Fig. 3-2 (b) condition with the HES approach using a VHM grid of 48 × 24. Top: Nondimensional space potential distribution. Bottom: Vector map of nondimensional velocity.

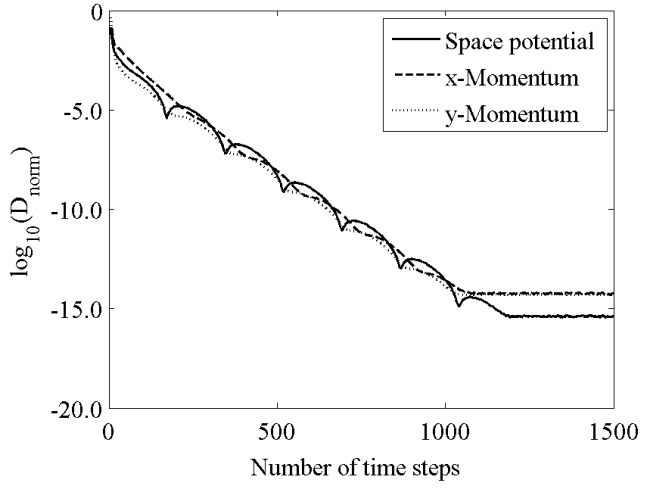

Figure 3-7: Time history of the normalized difference of each variable. The Fig. 3-2 (b) condition is solved with the HES approach using a 48 × 24 grid.

3.5 Computational cost comparison

The computation cost of the HES approach is compared with that of the EE approach. Order analyses of computation cost are conducted in terms of the size of the problem and the strength of magnetic confinement. The size of the problem is evaluated with the number of cells, N_{cell}, and the strength of magnetic confinement is associated with the ratio of electron mobility, $\mu_{||}/\mu_{\perp}$. Computation cost is measured with a sequential calculation without parallelization. The convergence is deemed to be satisfied when the normalized difference of the space potential reaches 10^{-10}, and the CPU second at convergence is termed T_{converge}.

Fig. 3-8 shows T_{converge} of the HES approach and the EE approach when the number of cells, N_{cell}, is varied. The computation time of the HES approach is $O\left(N_{\text{cell}}^{1.5}\right)$, whereas the cost of the EE approach is $O\left(N_{\text{cell}}^{1.8}\right)$. From this result, we conclude that the differences in computation time in terms of the size of the problem between the two approaches is insignificant. This fact supports the advantage of the HES approach in its ability to utilize a simple structured mesh without increasing computation time.

Fig. 3-9 shows a comparison of T_{converge} between the two approaches when the strength of magnetic confinement, $\mu_{||}/\mu_{\perp}$, is varied. The computation time of the EE approach increases with $\mu_{||}/\mu_{\perp}$, whereas that of the HES approach stays almost constant. This is because the eigenvalues of the system are always adjusted via Eq. (3.13) by the acceleration coefficient, and the condition number of the system does not increase with $\mu_{||}/\mu_{\perp}$ in the HES approach. This result indicates that the HES approach is suitable under conditions of strong anisotropy resulting from magnetic confinement. This is also an advantage of the HES approach.

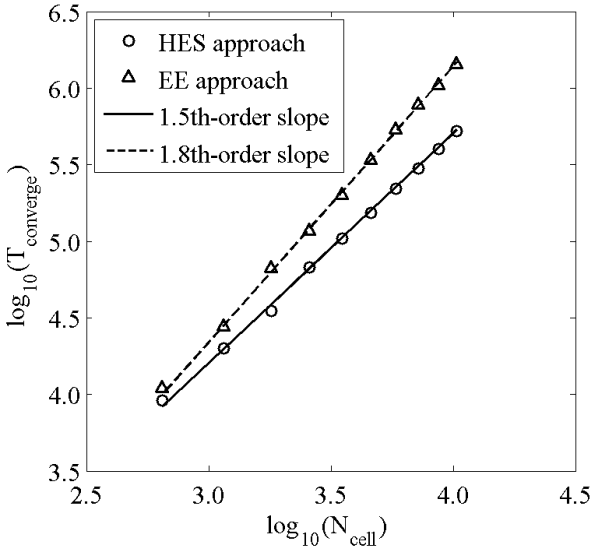

Figure 3-8: Computation costs until convergence when the number of cells is changed. The Fig. 3-2-(a) condition is solved using the HES approach and the EE approach. A logarithmic scale is used for each axis for scale analysis. 1.5th-, and 1.8th-order slopes are depicted for reference.

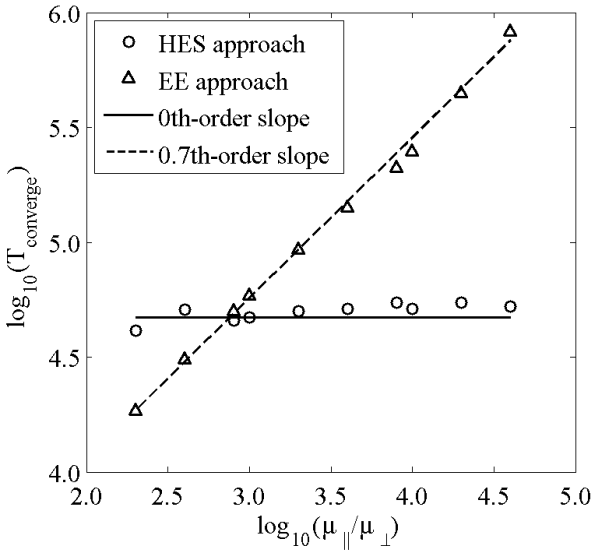

Figure 3-9: Computation costs until convergence when $\mu_{||}/\mu_{\perp}$ is changed. The Fig. 3-2-(a) condition is solved using the HES approach and EE approach. A logarithmic scale is used for each axis for scale analysis. Zeroth-, and 0.7th-order slopes are depicted for reference.

3.6 Comparison on mesh convergence of transverse electron flux

It is difficult to analyze the computational accuracy for anisotropic diffusion equations because the analytical solution is hard to be derived. Therefore, the mesh convergence of the calculated electron transverse flux is evaluated for the HES and EE approaches. Here the transverse electron flux is defined as the total electron flux flowing from the right to left side boundaries. The result is visualized in Fig. 3-10. The transverse electron fluxes calculated with a fine grid system are almost the same between the HES and EE approaches. However, with a coarse grid system, the transverse electron flux is overestimated in the HES approach. This indicates the HES approach has a large numerical viscosity stemming from the first-order upwind scheme. Thus, the HES approach should be used with schemes of high-order spatial accuracy for faster mesh convergence in practical calculations.

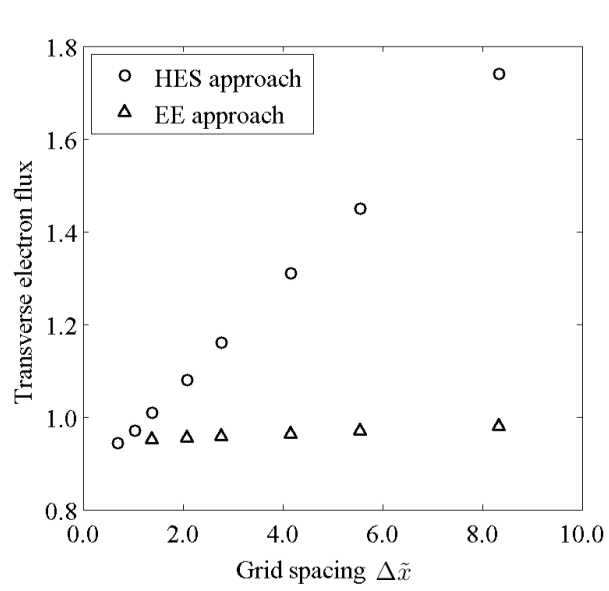

Figure 3-10: The transverse electron flux calculated by the HES and EE approaches when the grid spacing is varied. The Fig. 3-2-(a) condition is solved using the HES approach and EE approach.

3.7 Consideration on the pseudo-time advancement term

The test calculation results in Sec. 3.4 proved that the HES approach maintained numerical stability during the computation. The validity of intruducing the pseudo-time advancement terms into the mass and momentum conservation equations, is considered here. First, an implicit formulation of Eq. (2.22) can be written as follows:

$$n_{\mathrm{e}} \left[\mu\right] \nabla \phi^{n+1} - \left[\mu\right] \nabla \left(n_{\mathrm{e}} T_{\mathrm{e}}\right) = n_{\mathrm{e}} \vec{u}_{\mathrm{e}}^{n+1} = n_{\mathrm{e}} \vec{u}_{\mathrm{e}}^{n} + T_r \frac{\partial}{\partial t} \left(n_{\mathrm{e}} \vec{u}_{\mathrm{e}}\right)^n , \tag{3.26}$$

where T_r is the reference time. As described in Sec. 2.3, in collisional plasmas, the characteristic time scale governing the electron motion is electron-neutral collision. Thus, the choice of T_r as $T_r = \nu_{\mathrm{col}}^{-1}$ is reasonable, and eventually Eq. (3.5) is derived.

An analogy of the pseudo-compressibility method can be considered for the pseudo-time advancement term of space potential in the mass conservation equation. For clear expressions, the negative space potential is defined for negatively charged electrons:

$$\phi_{\mathrm{n}} = -\phi \tag{3.27}$$

Fig. 3-11 shows the concept of the analogy between the pseudo-time advancement term of space potential and pseudo-compressibility method. The effect of the space potential on the momentum conservation equation is similar to that of the pressure. The pseudo-compressibility method introduces a pseudo-time advancement term of pressure into the mass conservation equation.[22] This method stably and efficiently calculates incompressible and low speed flows, by using preconditioning methods.[38] Because of the similarity shown in Fig. 3-11, introducing a pseudo-time advancement term of space potential is supposed to yield a stable computation, in a mathematical sense. In addition, the coefficient of $n_{\mathrm{e}}/T_{\mathrm{e}}$ is added to the time-derivative term to arrange the dimension.

In the above discussion, the validity on the pseudo-time advancement term of

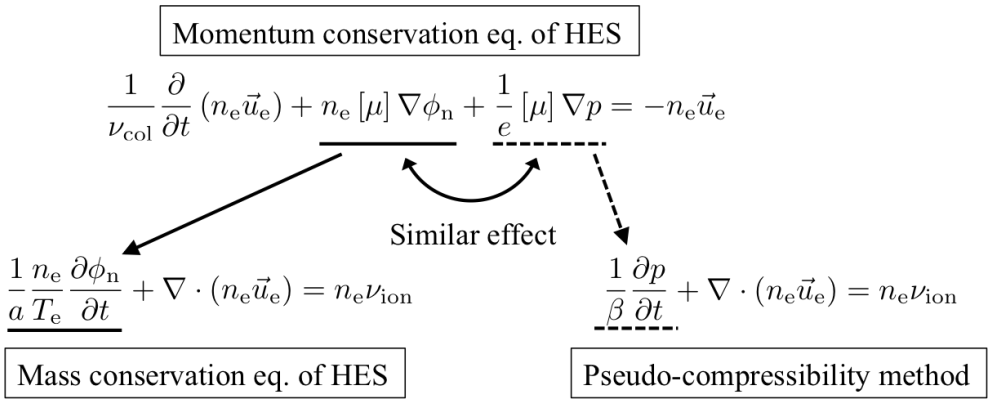

Figure 3-11: Analogy between pseudo-time advancement term of space potential and conventional pseudo-compressibility. β is a pseudo-compressibility parameter.

space potential is considered from the computational aspect. The physical aspect of the validity can be considered as follows. As explained in Sec. 2.4, under the plasma approximation, one needs to derive the space potential from the conservation equations of electron fluids. However, the space potential is originally determined by using the Gauss's law as follows:

$$\nabla^2\phi = -\frac{e}{\varepsilon_0}\left(n_{\mathrm{i}} - n_{\mathrm{e}}\right), \tag{3.28}$$

where ε_0 is the vacuum permittivity. If the ion number density is regarded as a time-constant quantity in the electron time scale, the space potential is basically dependent on only the electron number density. Therefore, it is supposed to be natural to replace the time-derivative term of electron number density in the mass conservation equation by the pseudo-time advancement term of the space potential. Further, by using the second-order central differencing, the discretized form of Eq. (3.28) can be written as follows:

$$\frac{1}{\Delta x^2}\left(\phi_{i-1,j} - 2\phi_{i,j} + \phi_{i+1,j}\right) + \frac{1}{\Delta y^2}\left(\phi_{i,j-1} - 2\phi_{i,j} + \phi_{i,j+1}\right) = \frac{e}{\varepsilon_0}\left(n_{\mathrm{e}} - n_{\mathrm{i}}\right). \tag{3.29}$$

In this equation, the sign of n_{e} in the right-hand side is positive, whereas the sign of $\phi_{i,j}$ in the left-hand side is negative. Thus, a pseudo-time advancement term of

negative space potential (ϕ_n) should be introduced in the mass conservation equation.

3.8 Improvement of preconditioning by using rotation matrix

The role of acceleration coefficients can be expanded to the preconditioning matrix. The system of equations of Eq. (3.14) can be rewritten using a preconditioning matrix as follows:

$$P^{-1}\frac{\partial Q}{\partial \tilde{t}} + J_x\frac{\partial Q}{\partial \tilde{x}} + J_y\frac{\partial U}{\partial \tilde{y}} = S, \tag{3.30}$$

where P is the preconditioning matrix. If only the three acceleration coefficients are considered, the preconditioning matrix is a diagonal matrix as follows:

$$P = \begin{pmatrix} a & & \\ & b_x & \\ & & b_y \end{pmatrix} = \begin{pmatrix} \sqrt{\frac{2}{\gamma}} & & \\ & \frac{\sqrt{2\gamma}}{\tilde{\mu}_x} & \\ & & \frac{\sqrt{2\gamma}}{\tilde{\mu}_y} \end{pmatrix}. \tag{3.31}$$

Based on the idea that the electron mobility tensor is derived by rotating the $[\mu]_{\text{mag}}$, a revised preconditioning matrix using a rotation matrix can be considered as follows:

$$\hat{P} = U^{-1}PU, \tag{3.32}$$

$$P = \begin{pmatrix} \sqrt{\frac{2}{\gamma}} & & \\ & \frac{\sqrt{2\gamma}}{\tilde{\mu}_{||}} & \\ & & \frac{\sqrt{2\gamma}}{\tilde{\mu}_{\perp}} \end{pmatrix}, \qquad U = \begin{pmatrix} 1 & & \\ & \cos\theta & \sin\theta \\ & -\sin\theta & \cos\theta \end{pmatrix}. \tag{3.33}$$

Preconditioning methods using rotation matrices are also used in CFD.[39] By using the revised preconditioning matrix $\hat{P}$, the flux Jacobian matrices are as simple as follows:

$$\hat{J}_x = \begin{pmatrix} 0 & -1 & 0 \\ -1 & 0 & 0 \\ 0 & 0 & 0 \end{pmatrix}, \qquad \hat{J}_y = \begin{pmatrix} 0 & 0 & -1 \\ 0 & 0 & 0 \\ -1 & 0 & 0 \end{pmatrix}. \tag{3.34}$$

Therefore, the Jacobian matrices become uniform throughout the calculation field without being affected by the magnetic field. The eigenvalues for these Jacobian matrices are the same as Eq. (3.17), and the advantage of smooth conveyance of information is maintained. The uniform Jacobian matrices enables the conservative form of the system of equations. Specifically, the system of equation can be rewritten as follows:

$$\frac{\partial U}{\partial \tilde{t}} + \frac{\partial}{\partial \tilde{x}}\left(\hat{J}_x U\right) + \frac{\partial}{\partial \tilde{y}}\left(\hat{J}_y U\right) = \hat{S}, \tag{3.35}$$

$$\hat{S} = \begin{pmatrix} 0 \\ -\frac{\sqrt{2\gamma}}{\tilde{\mu}_{||}}\left(\tilde{u}_x \cos^2\theta + \tilde{u}_y \cos\sin\theta\right) - \frac{\sqrt{2\gamma}}{\tilde{\mu}_{\perp}}\left(\tilde{u}_x \sin^2\theta - \tilde{u}_y \cos\sin\theta\right) \\ -\frac{\sqrt{2\gamma}}{\tilde{\mu}_{||}}\left(\tilde{u}_x \cos\sin\theta + \tilde{u}_y \sin^2\theta\right) + \frac{\sqrt{2\gamma}}{\tilde{\mu}_{\perp}}\left(\tilde{u}_x \cos\sin\theta - \tilde{u}_y \cos^2\theta\right) \end{pmatrix}. \tag{3.36}$$

Hence the effect of magnetic field is included in the source terms.

The test calculation condition of Fig. 3-2-(a) is computed by the formulation of Eq. (3.35). The calculation results in the steady state are presented in Fig. 3-13. As well as the results in Fig. 3-4, the dimensionless space potential distribution and electron streamlines reflect the effect of magnetic confinement. The convergence history of the variables are shown in Fig. 3-13. It is proved that the convergence history in Fig. 3-13 is smooth compared with that in Fig. 3-13. This is because the improved preconditioning of Eq. (3.33) contributes to further smooth information conveyance.

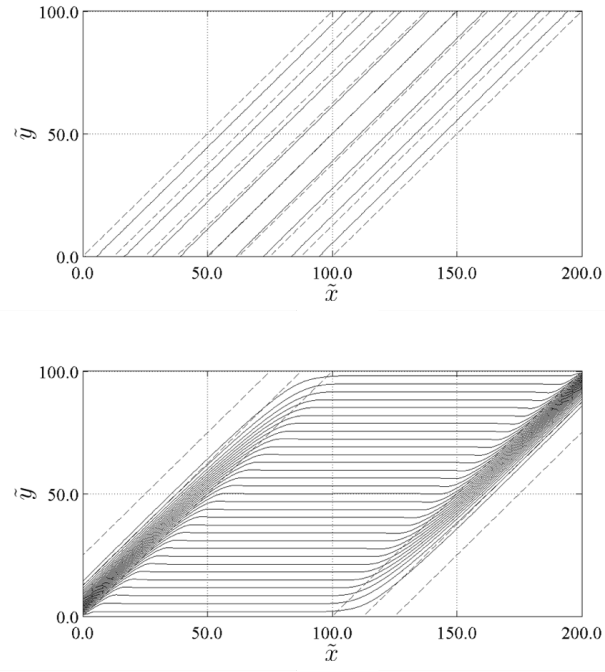

Figure 3-12: Calculation results for the Fig. 3-2-(a) condition with the HES approach using a VHM grid of 96 × 48. Top: Electron streamlines. Bottom: Vector map of nondimensional velocity. The dashed lines denote reference magnetic lines.

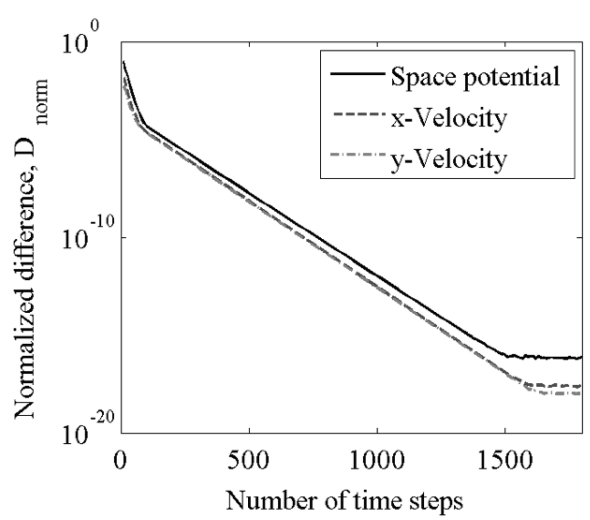

Figure 3-13: Time history of the normalized difference of each variable. The Fig. 3-2-(a) condition is solved with the HES approach using a 96 × 48 grid.

3.9 Summary of the chapter

A new approach using an HES is proposed for electron fluids in quasi-neutral plasmas. The main advantage of this approach is that it avoids cross-diffusion terms, which violate the diagonal dominance in conventional approaches using the EE. The HES approach enables robust calculations with a simple structured mesh such as a VHM by using an upwind scheme. Numerical experiments in two dimensions are conducted with angled magnetic lines of force to validate the HES approach. Furthermore, the computation time of the HES approach is compared with that of the MFAM-based EE approach. Also, the mesh convergence of transverse electron flux calculated by the two approaches are compared. Finally, the improvement of preconditioning matrix is presented. The findings are summarized as follows:

1. The calculation results computed by the HES approach reflect the effect of magnetic confinement and the given boundary conditions, and all pseudo-time advancement terms converge to negligibly small values. These facts validate the HES approach for electron fluids.

2. The computational cost of the HES approach is $O\left(N_{\mathrm{cell}}^{1.5}\right)$, whereas the cost of the EE approach is $O\left(N_{\mathrm{cell}}^{1.8}\right)$. The HES approach has an advantage that it can utilize a simple structured mesh without increasing computational cost.

3. With increasing $\mu_{||}/\mu_{\perp}$, the computational cost of the HES approach remains constant, whereas that of the EE approach increases. The HES approach is efficient in solving conditions of strong magnetic confinement.

4. The HES approach has a large numerical viscosity stemming from the first-order upwind scheme. The HES approach should be implemented with schemes of high-order spatial accuracy for good mesh convergence.

5. The preconditioning matrix is improved by using a rotation matrix. Very smooth convergence history can be obtained by the improved preconditioning.

Chapter 4

A flux-splitting method for the HES of electron fluids

In this chapter the hyperbolic-equation system (HES) approach is extended to the system including conservation equations of mass, momentum, and energy of electron fluids. A flux-splitting method is proposed for the HES in which the numerical fluxes are split into four categories. Furthermore, an upwind method which incorporates a flux-vector splitting (FVS) and advection upstream splitting method (AUSM) is proposed for upwinding the split numerical fluxes. The proposed method is applied to a test calculation condition of uniformly angled magnetic lines of force. A high-order space-accuracy scheme using the TVD-MUSCL technique is applied to the HES approach. All the pseudo-time advancement terms are monotonically convergent to negligibly small values. The calculation results are compared with those computed by an approach using an elliptic-parabolic equation system (EPES) with an magnetic-field-aligned mesh (MFAM). They are in good agreement in both qualitative and quantitative comparisons. This fact indicates the HES approach with the flux-splitting method achieves the computational accuracy of the same level of the approach using an MFAM.

4.1 An HES for energy conservation equation

The HES discussed in Chapter 3 consists of only mass and momentum conservation equations. To simulate plasma devices using the heating of electrons for plasma generation, an HES must include the energy conservation equation for deriving the electron temperature. As described in Sec. 2.5, the equation of energy conservation is formulated as follows:

$$\frac{\partial}{\partial t}\left(\frac{3}{2}n_{\mathrm{e}}T_{\mathrm{e}}\right)+\nabla\cdot\left(\frac{5}{2}n_{\mathrm{e}}T_{\mathrm{e}}\vec{u}_{\mathrm{e}}-\frac{5}{2}n_{\mathrm{e}}T_{\mathrm{e}}\left[\mu\right]\nabla T_{\mathrm{e}}\right)=n_{\mathrm{e}}\vec{u}_{\mathrm{e}}\cdot\nabla\phi-\alpha\varepsilon_{\mathrm{ion}}n_{\mathrm{e}}\nu_{\mathrm{ion}}. \quad (4.1)$$

The left-hand side consists of time derivative term, enthalpy convection term, and thermal diffusion term. The right-hand side is Joule heating and energy losses due to ionization, excitation and radiation.

4.1.1 Conservative form of energy conservation equation

By using the negative potential $\phi_{\mathrm{n}}=-\phi$ for the negative charge of electrons, the Joule heating term is converted as follows:

$$n_{\mathrm{e}}\vec{u}_{\mathrm{e}}\cdot\nabla\phi=-\nabla\cdot\left(n_{\mathrm{e}}\phi_{\mathrm{n}}\vec{u}_{\mathrm{e}}\right)+\phi_{\mathrm{n}}n_{\mathrm{e}}\nu_{\mathrm{ion}}. \quad (4.2)$$

In deriving Eq. (4.2), the equation of continuity of Eq. (2.17) is used. In the right-hand side of Eq. (4.2), the meanings of the first and second terms can be interpreted as the potential energy flow, and potential energy generation associated with electron generation, respectively. By using this relation, Eq. (4.1) can be rewritten as follows:

$$\frac{\partial}{\partial t}\left(\frac{3}{2}n_{\mathrm{e}}T_{\mathrm{e}}\right)+\nabla\cdot\left(\frac{5}{2}n_{\mathrm{e}}T_{\mathrm{e}}\vec{u}_{\mathrm{e}}-\frac{5}{2}n_{\mathrm{e}}T_{\mathrm{e}}\left[\mu\right]\nabla T_{\mathrm{e}}+n_{\mathrm{e}}\phi_{\mathrm{n}}\vec{u}_{\mathrm{e}}\right)=\left(\phi_{\mathrm{n}}-\alpha\varepsilon_{\mathrm{ion}}\right)n_{\mathrm{e}}\nu_{\mathrm{ion}}. \quad (4.3)$$

Therefore, the energy conservation equation can be expressed in a conservative form, and the conservation of fluxes can be strictly calculated by using a finite volume method (FVM). All of the source terms are associated with the electron generation.

4.1.2 Introduction of new variables for energy diffusion

The thermal diffusion term contains the mobility tensor in its coefficient, and hence this term causes anisotropic diffusion including the effect of cross diffusion. Because cross diffusion terms induce instabilities as explained in Sec. 3.1, an HES must be constructed for Eq. (4.3) New variables can be chosen arbitrarily if it contains the gradient of electron temperature. Here new variables $\vec{g}$ are defined as follows:

$$\vec{g} = -\left[\mu\right]\nabla T_{\mathrm{e}}. \tag{4.4}$$

Substituting Eq. (4.4) into Eq. (4.3) yields a hyperbolic equation as follows:

$$\frac{\partial}{\partial t}\left(\frac{3}{2}n_{\mathrm{e}}T_{\mathrm{e}}\right) + \nabla\cdot\left(\frac{5}{2}n_{\mathrm{e}}T_{\mathrm{e}}\vec{u}_{\mathrm{e}} + \frac{5}{2}n_{\mathrm{e}}T_{\mathrm{e}}\vec{g} + n_{\mathrm{e}}\phi_{\mathrm{n}}\vec{u}_{\mathrm{e}}\right) = \left(\phi_{\mathrm{n}} - \alpha\varepsilon_{\mathrm{ion}}\right)n_{\mathrm{e}}\nu_{\mathrm{ion}}. \tag{4.5}$$

This equation no longer contains diffusion terms and it can be regarded as a hyperbolic equation. Concerning the new variables $\vec{g}$, pseudo-time advancement terms are added to Eq. (4.4) as follows:

$$\frac{1}{\nu_{\mathrm{col}}}\frac{\partial\vec{g}}{\partial t} + \left[\mu\right]\nabla T_{\mathrm{e}} = -\vec{g}, \tag{4.6}$$

where ν_{col} is total collision frequency which is used as a reference time scale. Here an acceleration coefficient is omitted from Eq. (4.6) for simplicity. The variables $\vec{g}$ have the dimension of velocity. Thus, the meaning of $\vec{g}$ is the velocity of energy diffusion regarding a pseudo time. Originally, the characteristic speed of diffusion terms are infinite.[40] The introduction of the pseudo-time advancement term split the infinite speed of information into finite ones, with time step intervals of the pseudo time.

When one calculates only the energy conservation equation, an HES consisting of Eqs. (4.5) and (4.6) can be used. However, in order to calculate n_{e}, $\vec{u}_{\mathrm{e}}$, and T_{e}, the HES for full conservation equations is considered. By combining the HES of Eqs. (3.4) and (3.5), and the HES of Eqs. (4.5) and (4.6), the HES for full conservation equations can be constructed as follows:

$$\frac{n_{\mathrm{e}}}{T_{\mathrm{e}}}\frac{\partial\phi_{\mathrm{n}}}{\partial t} + \nabla\cdot\left(n_{\mathrm{e}}\vec{u}_{\mathrm{e}}\right) = n_{\mathrm{e}}\nu_{\mathrm{ion}}, \tag{4.7}$$

$$\frac{1}{\nu_{\rm col}}\frac{\partial}{\partial t}\left(n_{\rm e}\vec{u}_{\rm e}\right)+n_{\rm e}\left[\mu\right]\nabla\phi_{\rm n}+\left[\mu\right]\nabla\left(n_{\rm e}T_{\rm e}\right)=-n_{\rm e}\vec{u}_{\rm e}, \tag{4.8}$$

$$\frac{\partial}{\partial t}\left(\frac{3}{2}n_{\rm e}T_{\rm e}\right)+\nabla\cdot\left(\frac{5}{2}n_{\rm e}T_{\rm e}\vec{u}_{\rm e}+\frac{5}{2}n_{\rm e}T_{\rm e}\vec{g}+n_{\rm e}\phi_{\rm n}\vec{u}_{\rm e}\right)=\left(\phi_{\rm n}-\alpha\varepsilon_{\rm ion}\right)n_{\rm e}\nu_{\rm ion}, \tag{4.9}$$

$$\frac{1}{\nu_{\rm col}}\frac{\partial\vec{g}}{\partial t}+\left[\mu\right]\nabla T_{\rm e}=-\vec{g}. \tag{4.10}$$

Totally the system consists of six equations in two dimensions. Again the acceleration coefficients are omitted here since the optimization of the preconditioning matrix is considered in Sec. 4.2.

4.2 Issues of the HES for full conservation equations

For the computation of the HES, an upwind method based on an approximate Riemann solver should be used to make the numerical viscosity small. Especially, the approximate Riemann solvers using the characteristics of the system enable stable calculation with least numerical viscosity.

However, there is an issue when one considers an approximate Riemann solver based on the flux Jacobian matrices. The flux Jacobian matrices are too complicated to analyze the eigen-structure. Without the eigen-structure, it is difficult to diagonalize the Jacobian matrices. This issue is also reported when the first-order system approach is applied to the Navier-Stokes equation.[20] It is possible to calculate the HES consisting of Eq. (4.7) and Eq. (4.8), and the HES including Eq. (4.9) and Eq. (4.10), iteratively. However, the iterative calculation will result in a sluggish convergence because of the disparity between the characteristic speeds of the two systems. It is desired to compute the full conservation equations as a single system.

One approach to calculate a complicated system is to use an approximate Riemann solver which does not need the eigen-structure. For example, the Lax-Friedrichs scheme is usually used for ideal MHD equations.[41,42] (Even though the eigen-structure of the ideal MHD equation is analyzed,[43] the Lax-Friedrichs method is used for numerical stability.) However, it is known that the Lax-Friedrichs scheme has a large numerical viscosity. As is decribed in Sec. 3.6, the HES approach for anisotropic

diffusion equations originally contains a large numerical viscosity arising from the cross-diffusion terms. Thus, the Lax-Friedrichs scheme should not be used to avoid excessive numerical viscosities.

4.3 Flux-splitting method (deleted)

To be compliant with the “Guideline on Publication of Summary of Dissertation," this section is deleted.

4.4 Calculation Conditions and Numerical Methods (deleted)

To be compliant with the “Guideline on Publication of Summary of Dissertation," this section is deleted.

4.5 Convergence history of normalized differences (deleted)

To be compliant with the “Guideline on Publication of Summary of Dissertation," this section is deleted.

4.6 Steady-state calculation results (deleted)

To be compliant with the “Guideline on Publication of Summary of Dissertation," this section is deleted.

4.7 Mesh convergence of transverse electron flux and electron heat flux (deleted)

To be compliant with the “Guideline on Publication of Summary of Dissertation," this section is deleted.

4.8 Applicability to condition of complicated magnetic lines of force (deleted)

To be compliant with the “Guideline on Publication of Summary of Dissertation," this section is deleted.

4.9 Summary of the chapter

The HES was constructed for the conservation laws of magnetized electron fluids in quasi-neutral plasmas. The hyperbolic-equation system is calculated as a time-development problem by introducing pseudo-time advancement terms. To construct a robust upwind method based on the approximate Riemann solver for the HES, the flux-splitting method was proposed. The fluxes were split into four categories for which the upwind method incorporating the FVS and AUSM was used. The HES approach with the flux-splitting method was tested by using the calculation condition in which the magnetic lines of force were uniformly distributed and at 45° relative to the horizontal direction. The findings are summarized as follow:

1. All pseudo-time advancement terms converge monotonically to negligibly small values. This fact validates the robustness of the flux-splitting method and that the conservation equations are strictly satisfied.

2. The numerical viscosity is drastically reduced by using the high-order scheme, which results in better reflection of the magnetic confinement.

3. The calculation results obtained by using the HES approach with the flux-splitting method are identical to the results obtained by using the MFAM-based EPES approach, in both qualitative and quantitative comparisons. This fact indicates that a good computational accuracy can be obtained by using the HES approach, even with the use of a simple structured mesh.

4. The HES approach with the flux-splitting method was also applied to the condition of lens-shape magnetic lines of force. The calculation results are reasonable and it is proved that the HES approach with the flux-splitting method is applicable to the conditions of nonuniform magnetic field geometry.

Chapter 5

Application of HES approach to Hall thruster analyses

This chapter discusses the applicability of the HES approach to Hall thruster calculations. The HES approach is applied to an axial-radial two-dimensional calculation of a Hall thruster using the hybrid particle-in-cell (PIC) method. The applicability is examined by the following points: 1) conservation of electron flux, 2) satisfaction of Bohm criterion, and 3) the Boltzmann relation along magnetic lines of force in the region of strong magnetic confinement. Concerning point 1), strict conservations of numerical fluxes are expected by computing the HES by using the finite volume method. The point 2) evaluates how accurately the boundary condition of the wall sheath is implemented in the HES approach. The point 3) is expected if the HES approach reasonably calculates the magnetized electron fluid in Hall thrusters. The discussion is mainly focused on the verification, but not the validation.[48] Thus, simplified models are used for electron mobility and wall sheath, without losing the main characteristics of the Hall thruster discharge.

5.1 Hybrid PIC method using HES approach

In this chapter, the hybrid particle-in-cell (PIC) method is employed for the analyses of a Hall thruster. First of all, the use of hybrid PIC method is validated by considering the Knudsen number. In the cases of Hall thrusters, if the channel length is used for L, $Kn \sim 10$ for ions and neutrals, whereas $Kn \sim 0.1$ for electrons. From this analysis, it is obvious that ion and neutral flows should be calculated with the kinetic model. Concerning electrons, electrons are drifting in the azimuthal direction because of the Hall effect, and the representative length for electrons is supposed to be much longer than the channel length. Therefore, the fluid model for electrons is considered to be valid.

There have been a lot of numerical simulations using the hybrid PIC method for Hall thrusters, and it seems that there are two streams. One stream is that the electron fluid is calculated in an ordinary boundary-fitted mesh.[11,16,31,49] The hybrid PIC method using the HES approach is categorized in this stream. In contrast to the conventional works using the elliptic equation and parabolic equation, an accurate and efficient calculation is expected by using the HES approach.

The other stream is the approach using the so-called "quasi-one-dimensional model," which is originally proposed by Fife.[13] This code was improved to include various physics and the recent code was termed as HPHall-2.[10] In this model, the one-dimensional MFAM is constructed, and the one-dimensional conservation equations in the perpendicular direction of magnetic lines of force are calculated. The distributions along magnetic lines of force are determined based on the isothermal property and the Boltzmann relation.

Herein the hybrid PIC method using the HES approach is named as "HP-HES." The features of the HP-HES are compared with other modeling works in Table 5.1. The Hall2De[6] code is also listed in the table because it has a feature of the use of two-dimensional MFAM. The main purpose of the HP-HES code is accurate and efficient calculation of Hall thrusters, by using the simple structured boundary-fitted mesh (BFM).

Table 5.1: Summary of the HP-HES, HPHall-2, and Hall2De. BFM: Boundary-fitted mesh. MFAM: Magnetic-field-aligned mesh.

	HP-HES	HPHal-2[10]	Hall2De[6]
Developer	UT	UPM and MIT	JPL
Plasma model	Hybrid PIC	Hybrid PIC	Fully fluid
Electron sub-model	2-D calc.	“Quasi 1-D model"	2-D calc.
Electron sub-model mesh	2-D BFM	1-D MFAM	2-D MFAM

5.2 Physical models in the hybrid PIC method (deleted)

To be compliant with the “Guideline on Publication of Summary of Dissertation," this section is deleted.

5.3 Numerical method (deleted)

To be compliant with the “Guideline on Publication of Summary of Dissertation," this section is deleted.

5.4 Calculation condition (deleted)

To be compliant with the “Guideline on Publication of Summary of Dissertation," this section is deleted.

5.5 Results and discussion (deleted)

To be compliant with the “Guideline on Publication of Summary of Dissertation," this section is deleted.

5.6 Summary of the chapter

The HES approach was applied to the calculation of a Hall thruster using the hybrid PIC method. The HES approach is able to calculate the two-dimensional conservation equations of magnetized electron fluid with a simple structured mesh. The SPT-100 thruster was assumed as the calculation condition in which the simple models of electron mobility and electrostatic sheath were used. The findings are summarized as follows:

1. The hybrid PIC method using the HES approach is able to reproduce the fundamental characteristics of the Hall thruster discharge.

2. Electron fluxes are strictly conserved in the HES approach during the calculation of the hybrid PIC method.

3. The Bohm criterion was satisfied at the plasma-sheath boundary in front of the channel walls. This fact indicates that the HES approach accurately reflects the boundary conditions of the wall sheath to the plasma dynamics.

4. The Boltzmann relation along magnetic lines of force was confirmed in the strong magnetic confinement region. The HES approach reasonably calculates the magnetized electron fluid in the Hall thruster with simple rectangular mesh.

Based on the findings above, it is concluded that the HES approach is applicable to Hall thruster simulations using the hybrid PIC method, where the boundary condition of the sheath model is accurately implemented.

For practical numerical analyses of Hall thrusters, update of the models through validations are necessary. A lot of experimental data are available for the SPT-100 thruster, and validations from various aspects are envisaged. To make the calculation results reflect the experimental data, the electron mobility model may need tunings as well as the previous numerical simulations.[28,55] The calculation field is supposed to be expanded to further outer regions of the channel.

Once the model validation is implemented, the PIC-fluid hybrid PIC code using the HES approach enables numerical analyses on many physical phenomena which

have been difficult if one uses conventional models. Here two topics are introduced. One topic is the numerical analysis of magnetically shielded thrusters. Since the HES approach does not need the use of MFAM, the HES approach can be easily applied to the complicated magnetic topology of magnetically shielded thrusters. Especially, the estimation of the effect of magnetic shielding for thruster with anode layer (TAL) is planned. An experimental study of magnetically shielded TAL has been conducted at the University of Tokyo.[63] The numerical analysis should support the understanding of the physics and the design optimizations.

The other topic is the electron fluid calculation in the axial-azimuthal coordinate. As described in Sec. 3.1, the computation using elliptic equations becomes unstable with the presence of cross-diffusion terms. In the electron fluid calculation in the axial-azimuthal coordinate, cross-diffusion terms arise owing to the E x B drift and diamagnetic drift. The HES approach is supposed to be beneficial to stabilize the computation by avoiding the effects of cross-diffusion terms. It is expected that the PIC-fluid hybrid model using the HES approach reproduce the azimuthal oscillation phenomena such as the electron cyclotron oscillation, and contribute to the understanding the electron anomalous transport across magnetic lines of force.

Chapter 6

Conclusion

In this dissertation, a new approach using a hyperbolic-equation system (HES) was proposed for electron fluids in quasi-neutral plasmas. The HES is calculated as a time-development problem by introducing pseudo-time advancement terms. The main advantage of this approach is that it avoids cross-diffusion terms which violate the diagonal dominance in conventional approaches using the elliptic equation (EE). The HES approach enables robust calculations with a simple structured mesh such as a vertical-horizontal mesh (VHM) by using an upwind method. Further, the speed of convergence is accelerated by using the preconditioning and efficient implicit methods.

The HES was extended to the full conservation laws of magnetized electron fluids. To construct a robust upwind method based on the characteristics of the HES, the flux-splitting method was proposed. In this method, the fluxes are split into four categories for which the upwind method incorporating the FVS and AUSM is used. To reduce the numerical viscosity arising in the discretization of the HES, the third-order TVD-MUSCL technique was adopted.

Finally, the HES approach was applied to the calculation of a Hall thruster using the hybrid PIC method. The SPT-100 thruster was assumed as the calculation condition in which the simple models of electron mobility and electrostatic sheath were adopted.

Several test calculations were conducted to verify the efficiency, accuracy, and applicability of the HES approach. The efficiency and accuracy were discussed through

the comparisons between the HES approach and the MFAM-based approaches. The applicability was evaluated through the Hall thruster calculation by examining if the HES approach could reproduce the fundamental characteristics of the plasma flow in Hall thrusters. The major findings are summarized as follows:

1. The calculation results computed by the HES approach reflect the effect of magnetic confinement and the given boundary conditions, and all pseudo-time advancement terms converge to negligibly small values. These facts validate the HES approach for magnetized electron fluids.

2. The computational cost of the HES approach is $O\left(N_{\mathrm{cell}}^{1.5}\right)$, whereas the cost of the EE approach is $O\left(N_{\mathrm{cell}}^{1.8}\right)$. The HES approach has an advantage that it can utilize a simple structured mesh without increasing computational cost.

3. With increasing $\mu_{\|}/\mu_{\perp}$, the computational cost of the HES approach remains constant, whereas that of the EE approach increases. The HES approach is efficient in solving conditions of strong magnetic confinement.

4. The calculation results obtained by using the HES approach with the flux-splitting method are identical to the results obtained by using the MFAM-based elliptic-parabolic equation system (EPES) approach, in both qualitative and quantitative comparisons. This fact indicates that a good computational accuracy can be obtained by using the HES approach, even with the use of a simple structured mesh.

5. The HES approach with the flux-splitting method is applicable to the conditions of complicated magnetic field geometry.

6. The hybrid PIC method using the HES approach is able to reproduce the fundamental characteristics of the Hall thruster discharge.

7. In the Hall thruster calculation, the Bohm criterion was satisfied at the plasma-sheath boundary and the Boltzmann relation along magnetic lines of force was confirmed in the strong magnetic confinement region. These facts indicate that

the HES approach accurately calculates the plasma-sheath interaction and magnetized electron fluid in Hall thrusters with simple structured mesh.

Based on the findings above, the efficiency, accuracy, and applicability of the HES approach were verified in this dissertation.

Appendix A

Numerical methods of CFD

In this chapter, the numerical techniques of CFD used in this thesis are reviewed. Since the numerical techniques for the particle-in-cell (PIC) method can be referred in many numerical works of Hall thrusters,[64–66] this appendix focuses on the CFD techniques. Although most of the methods can be found on textbooks, some cautions are given when these methods are applied to the calculation of plasma flows and the HES approach. Verifications of the techniques are conducted, and the results are shown in Sec. A.10.

A.1 Conservative form and non-conservative form

In general, the partial differential equations of fluid conservation laws are expressed in either conservative form or non-conservative form. Conservative quantities are used in a conservative form. For instance, a set of two-dimensional equations in conservative form is expressed as follows:

$$\frac{\partial Q}{\partial t} + \frac{\partial E}{\partial x} + \frac{\partial F}{\partial y} + S = 0, \tag{A.1}$$

where Q, E, F, and S are a conservative quantity vector, x-flux vector, y-flux vector, and source term vector, respectively. The finite volume method (FVM) is usually used for solving the equations in the conservative form. In many shock-capturing schemes

used in CFD, the conservative form is preferred to satisfy the flux conservations between discontinuities of shock waves. On the other hand, a set of equations in non-conservative form is written as follows:

$$\frac{\partial U}{\partial t} + A\frac{\partial U}{\partial x} + B\frac{\partial U}{\partial y} + S = 0, \tag{A.2}$$

where U, A, and B are variable vector, x-Jacobian matrix, y-Jacobian matrix, respectively. If the set of equations is written in non-conservative form, it is difficult to apply the FVM because the numerical fluxes cannot be defined. Thus, the strict conservation of numerical fluxes is not expected with non-conservative forms.

In general, a conservative form and non-conservative form give different calculation results. It is said that if the solution is smooth and there is no discontinuity in the flow, the difference is small. However, if there is a discontinuity like a shock wave, only the conservative form yields physical results.[67] The conservative form is also preferred in computations of anisotropic flows such as magnetized electron fluids. Owing the the high anisotropy, a small residual in the computational may induce a large erroneous flux in one direction. Hence it is difficult to maintain the flux balance if one uses a non-conservative form.

A.2 Upwind method and flux vector splitting (FVS)

Upwind method for one-dimensional scalar hyperbolic equation

An one-dimensional scalar hyperbolic equation is considered as follows:

$$\frac{\partial u}{\partial t} + c\frac{\partial u}{\partial x} = 0, \tag{A.3}$$

where u is a scalar variable and c is time-independent quantity. Based on the sign of c, the upwind direction is determined. If one applies the first-order discretization for

time and space, the discretized equation in an explicit form is written as follows:

$$\frac{q_i^{n+1}-q_i^n}{\Delta t}+c\frac{q_i^n-q_{i-1}^n}{\Delta x}=0, \quad (c\geq 0)\,, \qquad \frac{q_i^{n+1}-q_i^n}{\Delta t}+c\frac{q_{i+1}^n-q_i^n}{\Delta x}=0, \quad (c<0)\,, \tag{A.4}$$

where n denotes time step, and i denotes cell number. Upwind method is known to be a stable approach for hyperbolic equations. The Courant-Friedrichs-Lewy (CFL) condition to stabilize the compuation is written as follows:

$$CFL \equiv |c|\frac{\Delta t}{\Delta x} < 1. \tag{A.5}$$

Basic concept of upwind method for system of equations

An one-dimensional system of equations is considered as follows:

$$\frac{\partial Q}{\partial t}+\frac{\partial E}{\partial x}=0. \tag{A.6}$$

Here Q is a variable vector and E is a flux vector. The Jacobian matrix can be defined as $A \equiv \partial E/\partial Q$ and Eq. (A.6) can be rewritten as follows:

$$\frac{\partial Q}{\partial t}+A\frac{\partial Q}{\partial x}=0. \tag{A.7}$$

With this form, it is difficult to define the upwind direction because A is a complicated matrix. So the technique of diagonalization is used as follows:

$$R^{-1}AR=\Lambda=\begin{bmatrix} c_1 & & \\ & \ldots & \\ & & c_m \end{bmatrix}; \qquad m: \text{number of equations (variables)}, \tag{A.8}$$

where R is eigenvector matrix and Λ is diagonal eigenvalue matrix. $c_1 \cdots c_m$ are the eigenvalues of A, which are also called characteristic speeds. By using the eigenstructure, Eq. (A.8) is rewritten as follows:

$$\frac{\partial Q}{\partial t}+R\Lambda R^{-1}\frac{\partial Q}{\partial x}=0. \tag{A.9}$$

Let's multiply R^{-1} from left-hand side of this equation, and define $\tilde{Q} \equiv R^{-1}Q$.

$$R^{-1}\frac{\partial Q}{\partial t} + \Lambda R^{-1}\frac{\partial Q}{\partial x} = 0. \Longleftrightarrow \frac{\partial \tilde{Q}}{\partial t} + \begin{bmatrix} c_1 & & \\ & \ldots & \\ & & c_m \end{bmatrix} \frac{\partial \tilde{Q}}{\partial x} = 0 \tag{A.10}$$

This conversion process is not very strict because R^{-1} is fixed on t and x. But Eq. (A.10) helps one to understand the concept of upwind method for a system of equations. Eq. (A.10) is just a set of scalar equations. So the upwind directions can be determined based on the signs of $c_1 \cdots c_m$, as well as the case of scaler hyperbolic equation.

Flux vector splitting (FVS)

The flux vector splitting (FVS) is one of the upwind approximate Riemann solvers.[34] The flow directions are determined by the signs of $c_1 \cdots c_m$. For instance in Eq. (A.6), the numerical flux flowing between the ith and $i+1$th cells is expressed as follows:

$$E_{i+\frac{1}{2}} = A_i^+ Q_i + A_{i+1}^- Q_{i+1}, \tag{A.11}$$

$$A^{\pm} = R\Lambda^{\pm}R^{-1}, \tag{A.12}$$

where Λ^+ and Λ^- consists of only positive and negative eigenvalues, respectively.

The FVS is an efficient upwind method compared with the Roe's flux difference splitting (FDS).[68] However, numerical fluxes become non-differentiable where the signs of eigenvalues change, which results in instabilities of the scheme. In order to avoid the non-differentiable points, another flux splitting using polynomial approximations is proposed.[69]

A.3 Advection upstream splitting method (AUSM)

The advection upstream splitting method (AUSM) is proposed to achieve the efficiency of FVS and the accuracy of FDS. This scheme also uses the polynomial ap-

proximations, and also, it simplifies the evaluation of numerical fluxes by separating the fluxes into advection ones and pressure ones. Let's think about an one-dimensional Euler equation as follows:

$$\frac{\partial Q}{\partial t} + \frac{\partial E}{\partial x} = 0, \tag{A.13}$$

where

$$Q = \begin{bmatrix} \rho \\ \rho u \\ e \end{bmatrix}, \qquad E = \begin{bmatrix} \rho u \\ \rho u u + p \\ h u \end{bmatrix}. \tag{A.14}$$

If the Jacobian for E is diagonalized, three eigenvalues of $u + a$, u, $u - a$ appear (a is the acoustic speed). The AUSM simplifies this problem by splitting the flux as,

$$E = \begin{bmatrix} \rho u \\ \rho u u + p \\ h u \end{bmatrix} = u \begin{bmatrix} \rho \\ \rho u \\ h \end{bmatrix} + \begin{bmatrix} \\ p \\ \\ \end{bmatrix} = Ma \begin{bmatrix} \rho \\ \rho u \\ h \end{bmatrix} + \begin{bmatrix} \\ p \\ \\ \end{bmatrix}, \tag{A.15}$$

where M is the Mach number. The upwind direction of the first flux can be determined by the sign of M. Furthermore, in the AUSM, the upwind direction of the second flux is also determined by the sign of M. The numerical flux is split into right- and left-running waves of information, as follows:

$$E = M^{+} a \begin{bmatrix} \rho \\ \rho u \\ h \end{bmatrix} + \begin{bmatrix} \\ p^{+} \\ \\ \end{bmatrix} + M^{-} a \begin{bmatrix} \rho \\ \rho u \\ h \end{bmatrix} + \begin{bmatrix} \\ p^{-} \\ \\ \end{bmatrix}. \tag{A.16}$$

Further, to avoid non-differentiable points, following polynomial approximations are used for the $-1 \leq M \leq 1$ region in the AUSM.

$$M^{\pm} = \begin{cases} \frac{1}{2}\left(M \pm |M|\right), & \text{if } |\mathrm{M}| > 1, \\ \pm\frac{1}{4}\left(M \pm 1\right)^2, & \text{otherwise}, \end{cases} \tag{A.17}$$

$$p^{\pm} = \begin{cases} \frac{1}{2}\left(1 \pm \text{sign}\left(M\right)\right), & \text{if } |\text{M}| > 1, \\ \frac{1}{4}\left(M \pm 1\right)^2 \left(2 \mp M\right), & \text{otherwise.} \end{cases} \tag{A.18}$$

The meaning of the polynomial approximation in Eqs. (A.17) and (A.18) are visualized in Figs. A-1 and A-2.

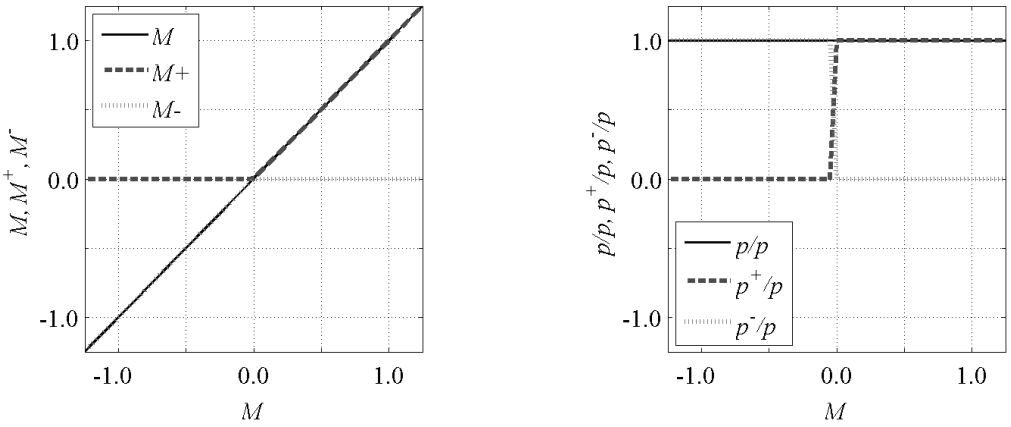

Figure A-1: Left: appearances of M^+ and M^- based on linear upwinding. Right: appearances of p^+/p and p^-/p based on the sign of M.

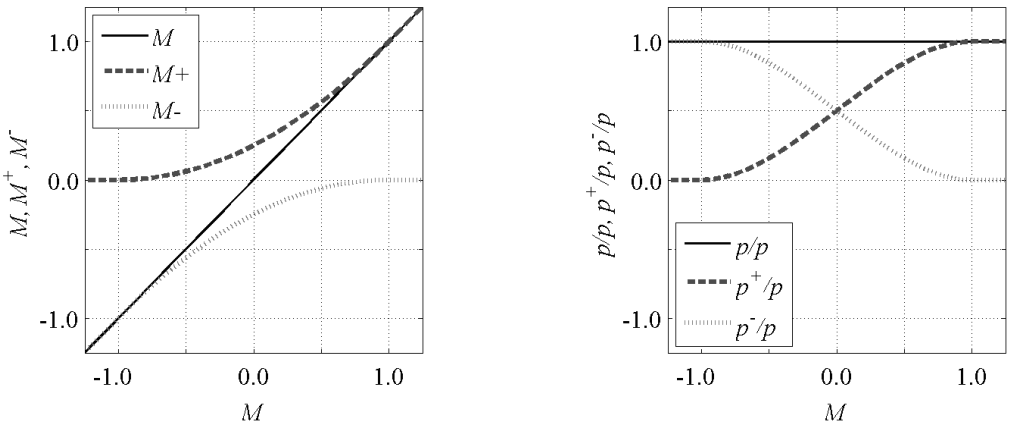

Figure A-2: Left: appearances of M^+ and M^- based on the polynomial approximation of Eq. (A.17), and right: appearances of p^+/p and p^-/p, based on the polynomial approximation of Eq. (A.18).

A.4 TVD-MUSCL

The total-variation diminishing monotone upstream scheme for conservation laws (TVD-MUSCL) is one of the most popular high-order space accuracy schemes because of its simplicity in implementations. The accuracy of the finite volume method (FVM) depends on the accuracy of the numerical fluxes flowing at the cell interfaces. These numerical fluxes are evaluated based on the flux Jacobian matrices and variables defined at the cell interfaces. The MUSCL is a kind of preconditioning methods to assess accurate quantities at the cell interfaces by using polynomial interpolations.

One can consider various distribution of quantities in computational cells such as the piecewise constant and piecewise linear distributions in Fig. A-3. The numerical fluxes are evaluated by the interpolated quantities. For example, the numerical flux flowing between the i th and $i+1$ th cells is calculated by using $u_{i+\frac{1}{2},L}$ and $u_{i+\frac{1}{2},R}$. By using the upwind MUSCL interpolation, these values are evaluated as follows:

$$\begin{aligned} u_{i+\frac{1}{2},L} &= u_i + \frac{1}{4}\Big((1-k)\,\Delta_- + (1+k)\,\Delta_+\Big)_i, \\ u_{i+\frac{1}{2},R} &= u_{i+1} - \frac{1}{4}\Big((1-k)\,\Delta_+ + (1+k)\,\Delta_-\Big)_{i+1}, \end{aligned} \tag{A.19}$$

where Δ is given by $(\Delta_+)_i = u_{i+1} - u_i$ and $(\Delta_-)_i = u_i - u_{i-1}$. The coefficient k determines the order of accuracy. A second-order accuracy is achieved by using $k = -1$, and a third-order accuracy is achieved by using $k = \frac{1}{3}$.

It is well known that the high-order schemes become unstable where the flow is complicated, if the MUSCL interpolation of Eq. (A.19) is directly applied. In order to regain the stability achieved by the first-order upwind method, the concept of TVD is applied. In the TVD-MUSCL, one just needs to introduce a nonlinear limiter function where the flow is not monotonic. The minmod limiter function is one of the most popular functions which contributes the stability of the scheme, and it is often used in plasma flow simulations.[42] This function is expressed as follows:

$$\tilde{\Delta}_+ = \mathrm{minmod}\left(\Delta_+, b\Delta_-\right), \qquad \tilde{\Delta}_- = \mathrm{minmod}\left(\Delta_-, b\Delta_+\right), \tag{A.20}$$

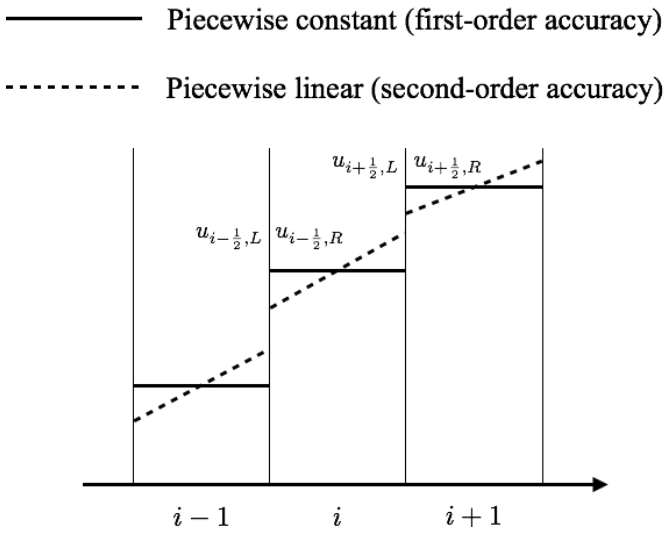

Figure A-3: Piecewise constant and piecewise linear distributions of quantity u in cells.

where the coefficient b is defined as follows:

$$b = \frac{3-k}{1-k}. \tag{A.21}$$

The TVD-MUSCL is derived by replacing $\Delta_{\pm}$ in Eq. (A.19) by $\tilde{\Delta}_{\pm}$.

A.5 Implicit method using delta-form

In many cases, only steady-state solutions are concerned and the transit until the steady state is out of interest. In this case, an implicit method should be used to avoid the Courant-Friedrichs-Lewy (CFL) restriction. In an implicit method, the flux is evaluated at the $n+1$ time level, and the time-derivative term of Eq. (A.6) can be discretized in the first-order form as

$$\Delta Q^n + \Delta t \left(\frac{\partial E}{\partial x}\right)^{n+1} = 0. \tag{A.22}$$

Here Δt is the time step interval and $\Delta Q^n \equiv Q^{n+1} - Q^n$. To linearize the flux in the direction of time, Beam and Warming proposed the following linearization method.[36]

$$E^{n+1} = E^n + \left(\frac{\partial E}{\partial Q}\right)^n \Delta Q^n + O\left(\Delta t^2\right). \tag{A.23}$$

If this linearization is used, by using the flux Jacobian vector of $A \equiv \partial E/\partial Q$, the Eq. (A.22) can be rewritten as,

$$\left(I + \Delta t \frac{\partial}{\partial x} A^n\right) \Delta Q^n = -\Delta t \left(\frac{\partial E}{\partial x}\right)^n. \tag{A.24}$$

Here the $\frac{\partial}{\partial x}$ in the left-hand side is also effective on ΔQ^n. Because A is a matrix, the left-hand side of Eq. (A.24) is a tridiagonal block operator. Thus, the calculation of the inverse of the operator can be easily implemented.

However, the situation is different in two- or three-dimensional calculations. For instance, the implicit form in two dimensions like Eq. (A.24) is written as follows:

$$\left(I + \Delta t \frac{\partial}{\partial x} A^n + \Delta t \frac{\partial}{\partial y} B^n\right) \Delta Q^n = -\Delta t \left(\frac{\partial E}{\partial x} + \frac{\partial F}{\partial y}\right)^n. \tag{A.25}$$

Here F is the flux in the y-direction and B is the flux Jacobian matrix of F. The configuration of the implicit matrix operator is illustrated in Fig. A-4. The coefficient matrix of the implicit operator becomes a wide-band matrix because two spatial indices (i, j) are involved. The matrix inverse calculation of the coefficient matrix needs a lot of computational time and machine memory. Therefore, efficient implicit methods for multi-dimensional calculations are developed as explained in the following sections.

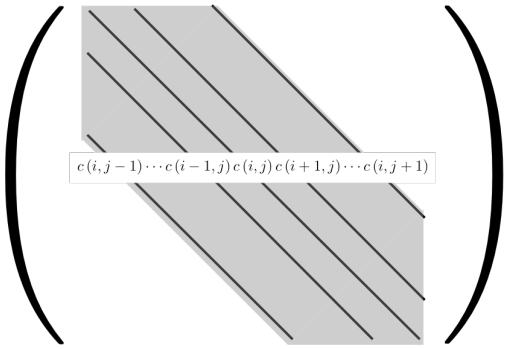

Figure A-4: The configuration of the coefficient matrix of the implicit operator of Eq. (A.25). c is the element of the coefficient matrix.

A.6 Lower-upper alternating direction implicit (LU-ADI) method

To avoid the calculation of matrix inversion of the complicated configuration like Fig. A-4, approximate factorizations are used. Eq. (A.25) can be modified by the alternating direction implicit (ADI) factorization proposed by Beam and Warming[36] as follows:

$$\left(I+\Delta t\frac{\partial}{\partial x}A^n+\Delta t\frac{\partial}{\partial y}B^n\right)\simeq\left(I+\Delta t\frac{\partial}{\partial x}A^n\right)\left(I+\Delta t\frac{\partial}{\partial y}B^n\right)+O\left(\Delta t^2\right). \quad \text{(A.26)}$$

The conceptual figure of this factorized operator is shown in Fig. A-5. The complicated configuration of the implicit operator is factorized into two tridiagonal block matrices by switching the indices. Therefore, the operator can be calculated by the two steps of inversion of tridiagonal block matrices as follows:

$$\left(I+\Delta t\frac{\partial}{\partial x}A^n\right)\Delta\vec{Q}^{n*}=-\Delta t\left(\frac{\partial\vec{E}}{\partial x}+\frac{\partial\vec{F}}{\partial y}\right)^n, \quad \text{(A.27)}$$

$$\left(I+\Delta t\frac{\partial}{\partial y}B^n\right)\Delta\vec{Q}^{n}=\Delta\vec{Q}^{n*}. \quad \text{(A.28)}$$

Furthermore, to enhance the diagonal dominance of the ADI-factorized operators, the lower-upper alternating direction implicit (LU-ADI) method was proposed.[37] This

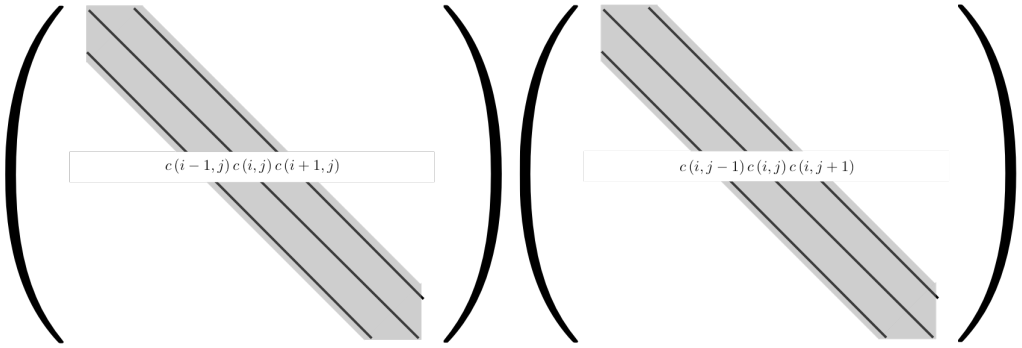

Figure A-5: The configuration of the implicit operator of Eq. (A.26). c is the element of the coefficient matrix. Each matrix is a tridiagonal block matrix.

method is known as a robust and fast multi-dimensional implicit method. The operator in x-direction is approximated by the lower-diagonal-upper (LDU) factorization as follows:

$$\left(I + \Delta t \frac{\partial}{\partial x} A^n\right) \simeq$$
$$\left(I - \frac{\Delta t}{\Delta x} A^{n-} + \Delta t \delta_x^b A^{n+}\right) \left(I + \frac{\Delta t}{\Delta x}\left(A^{n+} - A^{n-}\right)\right)^{-1} \left(I + \frac{\Delta t}{\Delta x} A^{n+} + \Delta t \delta_x^f A^{n-}\right) \quad \text{(A.29)}$$

where A^+ and A^- are the Jacobian matrices which contain only positive and negative eigenvalues, respectively. δ_x^f and δ_x^b are the forward and backward differences in x-direction, respectively. Totally six operators are involved in the LU-ADI method in two dimensions. Finally, a caution must be paid on the accuracy when the ADI method is used. ADI method has a numerical error of $O\left(\Delta t^2\right)$. This numerical error is trivial when a small Δt is used, because originally the first-order differencing is used for the time derivative. However, the numerical error becomes substantial when a large CFL is used, and the steady-state results can be distorted. Thus, a very large Courant number should be avoided even if the steady state is calculated stably. To the best of the author's knowledge, the Courant number exceeding 10^3 should not be used with the ADI method.

A.7 Lower-upper symmetric Gauss Seidel (LU-SGS) method

In addition to the LU-ADI method, the lower-upper symmetric Gauss Seidel (LU-SGS) method is commonly used as an efficient multi-dimensional implicit method.[45] The LU-SGS method uses the approximate LDU factorization as follows:

$$I + \Delta t \frac{\partial}{\partial x} A^n + \Delta t \frac{\partial}{\partial y} B^n = L + D + U, \tag{A.30}$$

$$L + D + U = (L + D) D^{-1} (D + U) + O\left(\frac{\Delta t^2}{1 + \Delta t}\right). \tag{A.31}$$

In one-dimensional cases, the structure of $(L + D) D^{-1} (D + U)$ is the same as the right-hand side of Eq. (A.29). Thus, the LU-ADI method can be understood as that it applies the LDU factorization after the ADI factorization.

The LDU-factorized matrix can be calculated by an iterative method. Let's consider solving an equation as follows:

$$(L + D) D^{-1} (D + U) \Delta Q = RHS. \tag{A.32}$$

For this equation, the two-step symmetric Gauss-Seidel method can be described as follows:

$$\begin{aligned} \text{Step1}: &\quad (L + D) \Delta Q^{n+1/2} = RHS^n, \\ \text{Step2}: &\quad (D + U) \Delta Q^{n+1} = -L \Delta Q^{n+1/2} + RHS^n. \end{aligned} \tag{A.33}$$

As written in Eq. (A.29), L, D, and U are described by the split Jacobian matrices such as $A^{\pm}$ and $B^{\pm}$. In the LU-SGS method, the split Jacobian matrices are roughly evaluated as follows:

$$A^{\pm} = \frac{1}{2} (A \pm \sigma \rho (A) I), \qquad B^{\pm} = \frac{1}{2} (B \pm \sigma \rho (B) I). \tag{A.34}$$

Here, ρ is the maximum spectral radius (maximum eigenvalue), and the parameter σ is usually set around 1.01. By introducing this approximation, D becomes a diagonal matrix. Therefore, $\Delta Q^{n+1/2}$ can be obtained by the forward calculation, and ΔQ^{n+1} can be obtained by the backward calculation. Because no matrix inversion calculation is involved, a vary rapid calculation is possible. It is noted that if D is originally diagonal matrix, the use of spectral radius is not necessary.

In the LU-ADI method, there is a limitation of the time step interval Δt due to the $O(\Delta t^2)$ error involved in the ADI factorization of Eq. (A.26). In the LU-SGS method, the error is $O(\Delta t)$ when a large Δt is used, and $O(\Delta t^2)$ when a small Δt is used. Thus, when a large Δt is used for a fast convergence, the error of the LU-SGS method is not predominant and is on the same order as the time-derivative term. This is an advantage of the LU-SGS method.

A.8 ADI-SGS method

One can consider the conbination of the LU-SGS method with the ADI factorization. After the ADI factorization of Eq. (A.26), the approximate LDU factorization can be applied as follow:

$$I + \Delta t \frac{\partial}{\partial x} A^n = L + D + U \simeq (L + D) D^{-1} (D + U) . \tag{A.35}$$

The matrix inversion calculation is replaced by the two-step sweep calculation of SGS method as written in Eq. (A.33). This method is known as the ADI-SGS method.[42]

The advantage of this scheme is that the vectorization and parallelization are easy because the operator in each direction can be calculated separately. Regarding the disadvantage, it is supposed that this method suffers a large numerical viscosity stemming from the ADI factorization and the introduction of the spectral radius for diagonal D.

A.9 Successive over relaxation (SOR) method

When one solves an elliptic equation as a boundary value problem, one needs to calculate a system of equations. The calculation methods for the system are categorized into two methods. One is the direct method which inverses the coefficient matrix. The other one is the iterative method which derive an approximate solution by decreasing the residuals. The successive over relaxation (SOR) method is a simple iterative method which is typically used for calculations of elliptic equations. The SOR method stably calculate multi-dimensional elliptic equation if the diagonal dominance of the coefficient matrix is satisfied.

For instance, let's think about a two-dimensional Poisson equation of Gauss's law as follow:

$$-\nabla^2\phi = \frac{\rho}{\varepsilon_0}, \tag{A.36}$$

where ϕ, ρ, and ε_0 are space potential, charge density, and permittivity of vacuum, respectively. Diffusion terms can be stably calculated by using the central differencing. Thus Eq. (A.36) can be discretized as follow:

$$-\frac{\phi_{i+1,j} - 2\phi_{i,j} + \phi_{i-1,j}}{\Delta x^2} - \frac{\phi_{i,j+1} - 2\phi_{i,j} + \phi_{i,j-1}}{\Delta y^2} = \frac{\rho_{i,j}}{\varepsilon_0} \tag{A.37}$$

$$\Longleftrightarrow \phi_{i,j} = \left(\frac{2}{\Delta x^2} + \frac{2}{\Delta y^2}\right)^{-1} \left(\frac{\rho_{i,j}}{\varepsilon_0} + \frac{\phi_{i+1,j} + \phi_{i-1,j}}{\Delta x^2} + \frac{\phi_{i,j+1} + \phi_{i,j-1}}{\Delta y^2}\right) \tag{A.38}$$

i are j are the indices in x-direction and y-direction of calculation mesh, respectively. The steady-state solution of ϕ is solved by iterative sweep calculations. If the sweep direction is $i : 1 \to N_\mathrm{x}$ and $j : 1 \to N_\mathrm{y}$, the SOR method can be formulated as follows:

$$\phi_{i,j}^{n+1} = \omega \left(\frac{2}{\Delta x^2} + \frac{2}{\Delta y^2}\right)^{-1} \left(\frac{\rho_{i,j}^{n}}{\varepsilon_0} + \frac{\phi_{i+1,j}^{n} + \phi_{i-1,j}^{n+1}}{\Delta x^2} + \frac{\phi_{i,j+1}^{n} + \phi_{i,j-1}^{n+1}}{\Delta y^2}\right) \tag{A.39}$$

Here, ω is the relaxation parameter which is chosen as $1 \leq \omega < 2$ to accelerate the calculation. When the diagonal dominance of the coefficient matrix is not strict, $\omega < 1$ is chosen for stable calculations. In this dissertation, ω is set at 1.8 in most cases.

A.10 Verification of numerical techniques

Test calculations are conducted to check if the numerical methods are coded appropriately. Basically in the process of verification, calculation results are compared to analytical solutions. Also, the mesh convergence is analyzed in steady state problems to check if the numerical error is decreasing with expected order of accuracy.

Verification of FVS, AUSM, and TVD-MUSCL

As a test problem let's consider a Poisson's equation as follows:

$$\frac{\partial^2 \phi}{\partial x^2} = A \cos\left(2\pi N \frac{x}{L}\right). \tag{A.40}$$

By introducing a new variable $u = \frac{\partial \phi}{\partial x}$, a hyperbolic-equation system (HES) can be constructed as follows:

$$\frac{\partial u}{\partial x} = A \cos\left(2\pi N \frac{x}{L}\right), \qquad \frac{\partial \phi}{\partial x} = u. \tag{A.41}$$

For this problem the analytical solutions for ϕ and u are derived as follows:

$$\phi = -\left(\frac{L}{2\pi N}\right)^2 A \cos\left(2\pi N \frac{x}{L}\right) + Bx + C, \tag{A.42}$$

$$u = \frac{L}{2\pi N} A \sin\left(2\pi N \frac{x}{L}\right) + B, \tag{A.43}$$

where B and C are constants of integration. The boundary conditions are given as follows:

$$\phi_{i=1} = \phi_{Anode}, \qquad \phi_{i=N} = \phi_{Cathode}. \tag{A.44}$$

Then, the constants of integration are expressed as follows:

$$B = \frac{\phi_{Cathode} - \phi_{Anode}}{L}, \qquad C = \left(\frac{L}{2\pi N}\right)^2 + \phi_{Anode}. \tag{A.45}$$

For test calculation, the following numbers are assumed in the calculation.

$$A = 10, \qquad L = 1, \qquad N = 3, \qquad \phi_{Anode} = 2, \qquad \phi_{Cathode} = 1. \tag{A.46}$$

The HES of Eq. (A.41) can be computed by the HES approach, as described in Sec. 3. Pseudo-time advancement terms are introduces into the system as follows:

$$\frac{\partial \phi}{\partial t} - \frac{\partial u}{\partial x} = -A \cos\left(2\pi N \frac{x}{L}\right), \qquad \frac{\partial u}{\partial t} - \frac{\partial \phi}{\partial x} = -u. \tag{A.47}$$

For this HES, the Jabobian matrix and the eigenvalues are written as follows:

$$J_x = \begin{pmatrix} 0 & -1 \\ -1 & 0 \end{pmatrix}, \qquad \lambda_x = \pm 1. \tag{A.48}$$

Based upon these Jacobian matrix and eigenvalues, the test problem can be computed by the FVS in Sec. A.2. Fig. A-6 shows the calculation results when the test problem is calculated by a first-order upwind method with a grid number of 96 and a Courant number of 0.02. u is calculated accurately, whereas ϕ has a lot of numerical viscosity. Fig. A-7 presents the results obtained by the first-order AUSM. The numerical viscosity in ϕ of the first-order FVS is slightly reduced. However, it is reported that the AUSM is unstable compared with the FVS, and the AUSM required greater computational time for convergence than the FVS. To reduce the numerical viscosity the TVD-MUSCL in Sec. A.4 is applied with the minmod limiter function. Fig. A-8 presents the results of the calculation when a second-order scheme is used. The numerical viscosity of ϕ in the result of fist-order approach is greatly reduced.

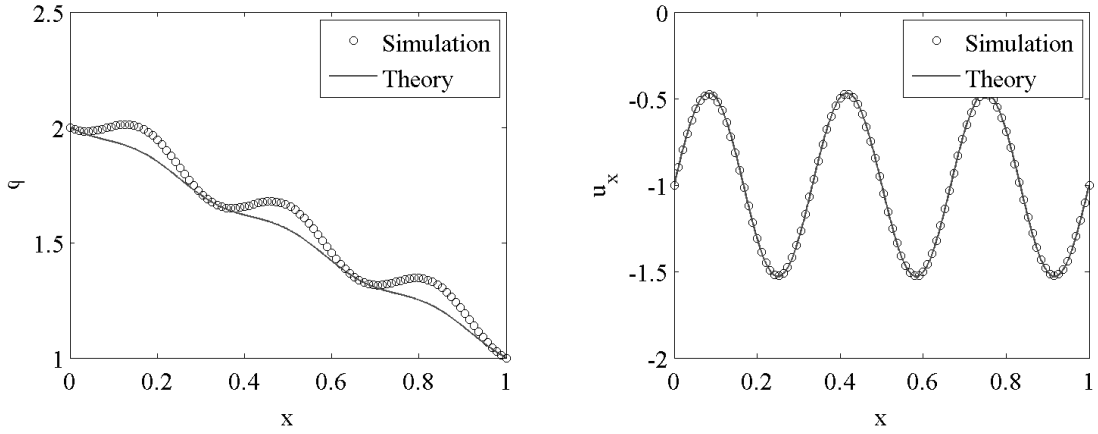

Figure A-6: Results of first-order upwind FVS. Left: ϕ. Right: u_x. Grid number is 96.

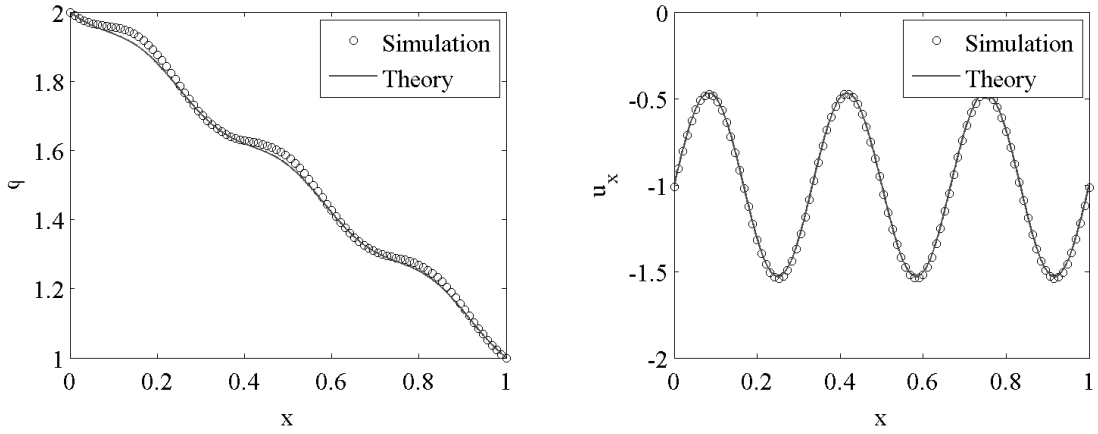

Figure A-7: Results of first-order AUSM. Left: ϕ. Right: u_x. Grid number is 96.

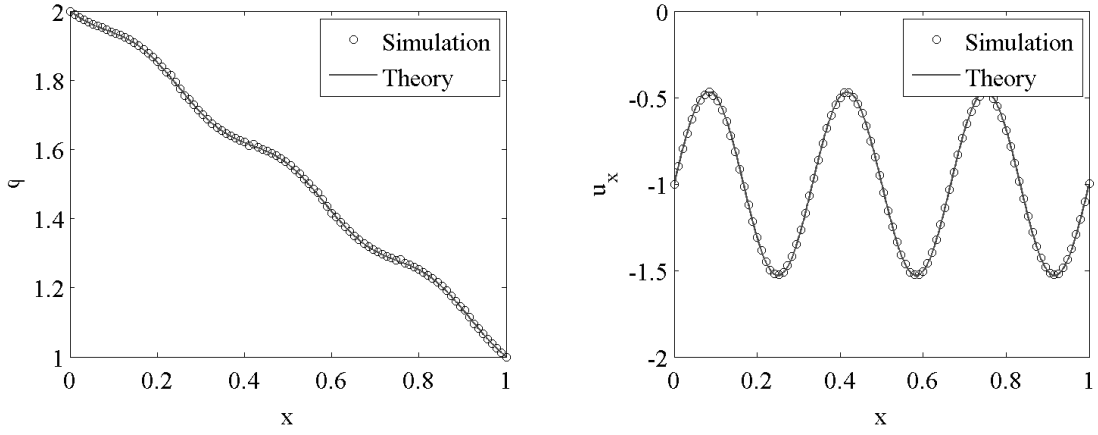

Figure A-8: Results of second-order TVD-MUSCL FVS. Left: ϕ. Right: u_x. Grid number is 96.

The order of accuracy can be checked by calculating the numerical errors with varying grid sizing. Here the normalized error is defined as follows:

$$E_{\mathrm{norm}} = \sqrt{\frac{1}{N_{\mathrm{cell}}} \sum^{N_{\mathrm{cell}}} \left(\frac{|y_{\mathrm{simulation}} - y_{\mathrm{theory}}|^2}{|y_{\mathrm{theory}}|^2 + \varepsilon} \right)}, \tag{A.49}$$

where ε is a tiny positive parameter satisfying $\varepsilon \ll |y|$ to avoid division by zero. It is noted that the numerical error treated herein is the discretization error. The machine error is neglected because it is negligibly small in typical calculation conditions.

Figs. A-9 and A-10 show the mesh convergences of ϕ and u, respectively, for first-order upwind method, second-order TVD-MUSCL, and third-order TVD-MUSCL. The errors are decreasing in all of the schemes. However, the order of accuracies differ from expected values, especially in the TVD-MUSCL. For instance, the order of accuracy attained by the second-order TVD-MUSCL is 2.70 for ϕ and 1.76 for u.

The discrepancy of the order of accuracies between the results and expected values is coming from the manner of MUSCL interpolation. In this test calculation, the MUSCL interpolation is implemented for characteristic variables, because the TVD-MUSCL is based on the scalar calculation. Instead of ϕ and u, the order of accuracy is checked for characteristic variable. For the hyperbolic system of Eq. (A.41), the characteristic quantities are written as follows:

$$q_1 = \frac{\phi - u}{2}, \qquad q_2 = \frac{\phi + u}{2}. \tag{A.50}$$

The mesh convergences of these characteristic quantities are shown in Figs. A-11 and A-12, respectively. The order of accuracies attained by the second-order TVD-MUSCL for q_1 and q_2 are 1.96 and 1.95, respectively. Thus, it is concluded that the TVD-MUSCL is implemented appropriately.

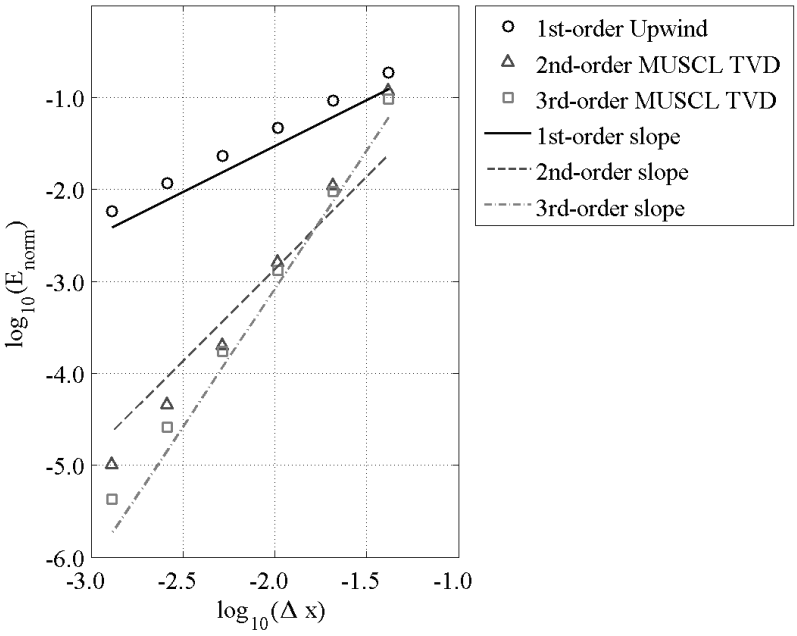

Figure A-9: Mesh convergence of ϕ. The order of accuracy for each scheme is estimated as 1st: 1.00, 2nd: 2.70, and 3rd: 2.88.

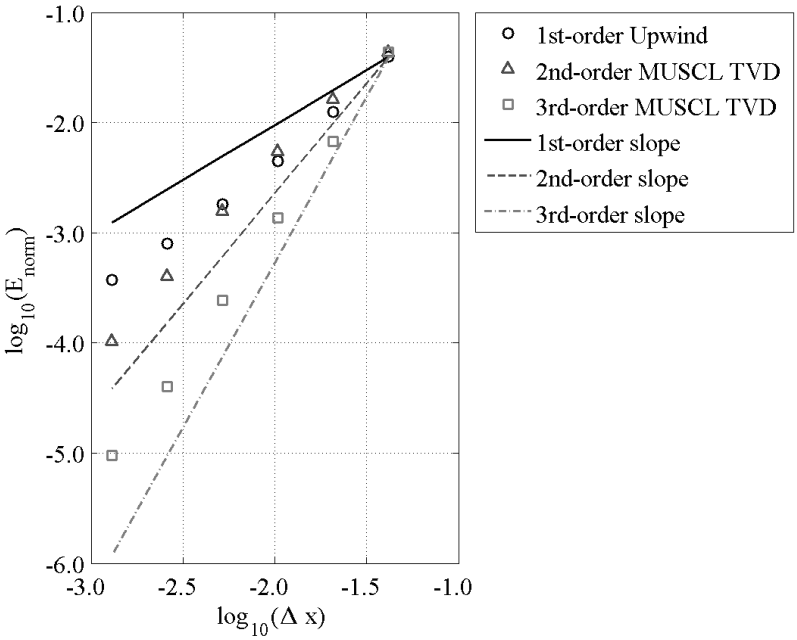

Figure A-10: Mesh convergence of u. The order of accuracy for each scheme is estimated as 1st: 1.34, 2nd: 1.76, and 3rd: 2.44.

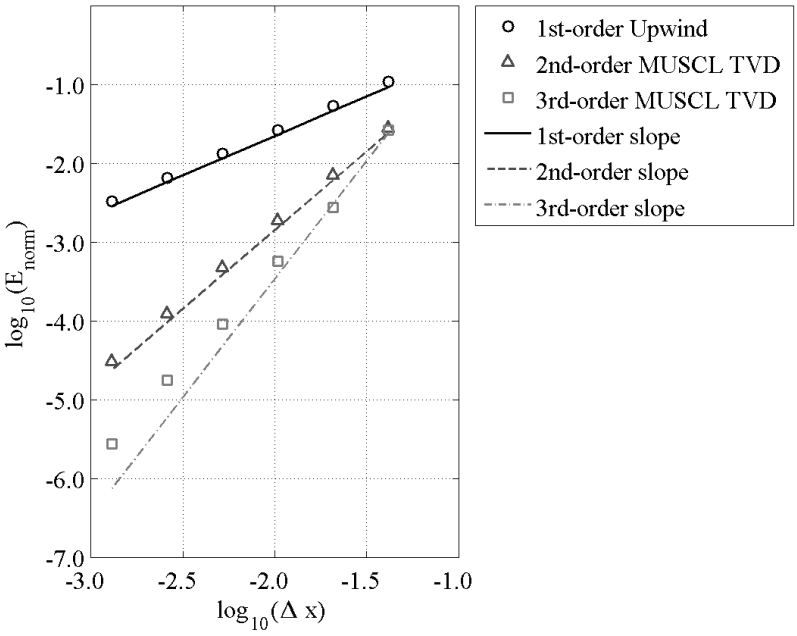

Figure A-11: Mesh convergence of q_1. The order of accuracy for each scheme is estimated as 1st: 1.01, 2nd: 1.96, and 3rd: 2.59.

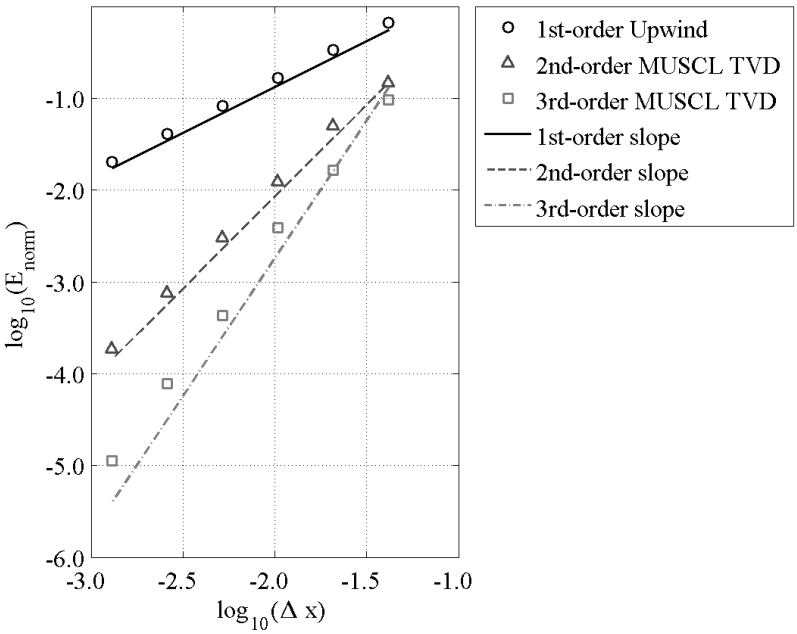

Figure A-12: Mesh convergence of q_2. The order of accuracy for each scheme is estimated as 1st: 1.01, 2nd: 1.95, and 3rd: 2.62.

Verification of implicit methods

Here the implicit methods for hyperbolic-equation systems are verified. The condition in Fig. 3-2-(a) is used for the test, and the HES of Eq. (3.14) is calculated. The Courant number is set at $CFL = 30$, for all of the calculations. The implicit methods of only Beam-Warming linearization, LU-ADI method, ADI-SGS method, and 6-core parallelized ADI-SGS method are implemented. The convergence is deemed to be satisfied when the normalized difference of the space potential reaches 10^{-10}, and the CPU second at convergence is termed T_{converge}.

Fig. A-13 shows the computational times of the implicit methods of only Beam-Warming linearization and LU-ADI method. First of all, the computations are stable for each method, even with $CFL = 30$. This gives a proof on the coding of the implicit methods. The computational time is greatly reduced in the LU-ADI method. The order of computational time is also decreased from $O\left(N_{\text{cell}}^3\right)$ to $O\left(N_{\text{cell}}^{1.5}\right)$. This reduction of computational time is mainly owing to the ADI factorization.

Furthermore, the computational times of LU-ADI method, ADI-SGS method, 6-core parallelized ADI-SGS are compared in Fig. A-14. Even though the order of computational time is not decreased, the computational time of the ADI-SGS method is approximately 1/5 of that of the LU-ADI method. This is mainly because of the characteristics of the Jacobian matrices in Eq. (3.16). Normally the SGS-type methods must introduce the spectral radius ρ to make D in the approximate LDU factorization diagonal. The use of the spectral radius induces a lot of numerical viscosities. However, if the Jacobian matrices in Eq. (3.16) are used, D becomes naturally diagonal without introducing ρ. Thus, very efficient calculations are expected with the SGS-type schemes.

Further reduction of computational time is confirmed in the six-core parallelized ADI-SGS method. The big advantage of the ADI-type method is the simplicity in the parallelization. Although the parallelization is "desperate" in the LU-SGS method,[70] the ADI method enables the segmentation of the region based on row and column.

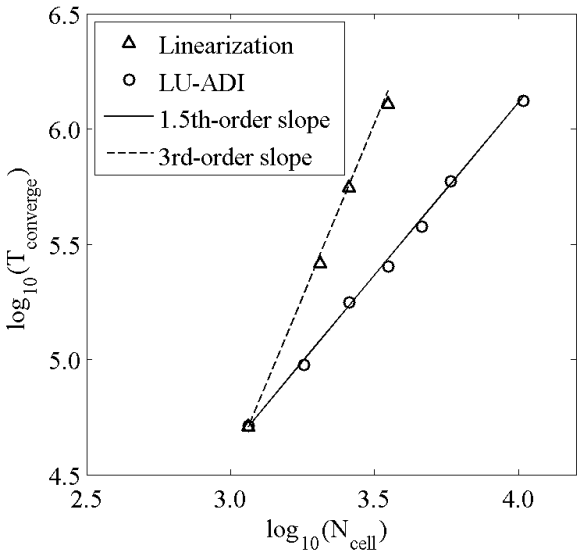

Figure A-13: Computation costs until convergence when the number of cells is changed. The Fig. 3-2-(a) condition is solved using the HES approach. Implicit methods of only Beam-Warming linearization and LU-ADI are implemented. A logarithmic scale is used for each axis for scale analysis. 1.5th-, and 3rd-order slopes are depicted for reference.

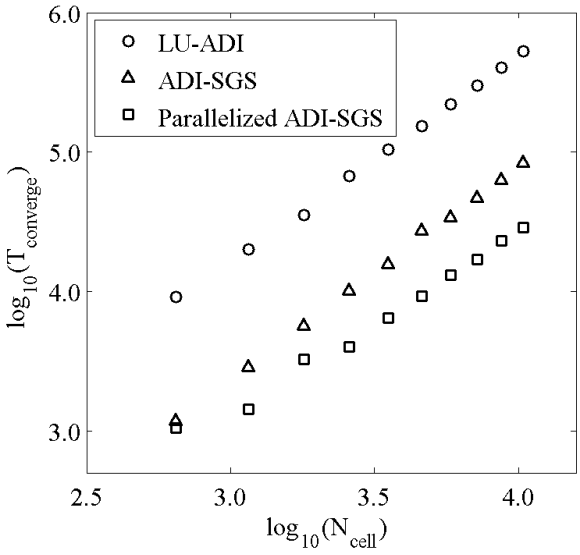

Figure A-14: Computation costs until convergence when the number of cells is changed. The Fig. 3-2-(a) condition is solved using the HES approach. Implicit methods of LU-ADI, ADI-SGS, six-core parallelized ADI-SGS are compared. A logarithmic scale is used for each axis for scale analysis.

Verification of elliptic equation solver

Elliptic equations are usually solved by applying central differencing and an iterative method. Here the Poisson's equation in Eq. (A.40) is calculated by using a second-order central differencing and the SOR method. The SOR method is implemented with a relaxation parameter of 1.8. The mesh convergence of the normalized error is visualized in Fig. A-15. The normalized error is decreasing with the order of $O(\Delta x^2)$ as expected by the theory.

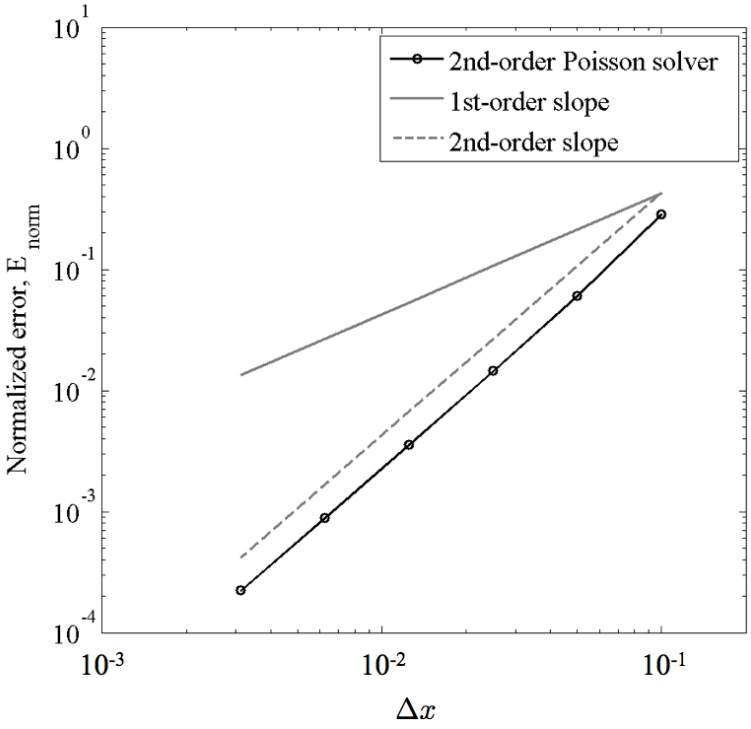

Figure A-15: Mesh convergence of normalized error. 2nd-order slope was derived by the 2nd-order Poisson's equation solver by the SOR method.

Bibliography

[1] Takahashi, T., Yamada, Y., Kondoh, Y., Goto, M., Okada, T., Hirano, Y., Asai, T., Takahashi, T., and Tomita, Y., "Hybrid simulation of neutral beam injection into a field-reversed configuration," *Journal of Plasma Physics*, Vol. 72, 12 2006, pp. 891–894.

[2] Kajimura, Y., Usui, H., Funaki, I., Ueno, K., Nunami, M., Shinohara, I., Nakamura, M., and Yamakawa, H., "Hybrid particle-in-cell simulations of magnetic sail in laboratory experiment," *Journal of Propulsion and Power*, Vol. 26, No. 1, 2010, pp. 159–166.

[3] Goebel, D. M. and Katz, I., *Fundamentals of Electric Propulsion: Ion and Hall Thrusters*, Johm Wiley & Sons, New Jersey, 2008.

[4] Cho, S., Komurasaki, K., and Arakawa, Y., "Kinetic particle simulation of discharge and wall erosion of a Hall thruster," *Physics of Plasmas*, Vol. 20, No. 6, 2013, pp. 063501.

[5] Garrigues, L., Hagelaar, G. J. M., Bareilles, J., Boniface, C., and Boeuf, J. P., "Model study of the influence of the magnetic field configuration on the performance and lifetime of a Hall thruster," *Physics of Plasmas*, Vol. 10, No. 12, 2003, pp. 4886 – 4892.

[6] Mikellides, I. G., Katz, I., Hofer, R. R., Goebel, D. M., de Grys, K., and Mathers, A., "Magnetic shielding of the channel walls in a Hall plasma accelerator," *Physics of Plasmas*, Vol. 18, No. 3, 2011, pp. 033501.

[7] Hofer, R. R., Goebel, D. M., Mikellides, I. G., and Katz, I., "Magnetic shielding of a laboratory Hall thruster. II. Experiments," *Journal of Applied Physics*, Vol. 115, No. 4, 2014, pp. 043304.

[8] Mikellides, I. G., Katz, I., Hofer, R. R., and Goebel, D. M., "Magnetic shielding of a laboratory Hall thruster. I. Theory and validation," *Journal of Applied Physics*, Vol. 115, No. 4, 2014, pp. 043303.

[9] Szabo, J., Warner, N., Martinez-Sanchez, M., and Batishchev, O., "Full Particle-In-Cell Simulation Methodology for Axisymmetric Hall Effect Thrusters," *Journal of Propulsion and Power*, Vol. 30, No. 1, 2013, pp. 197–208.

[10] Parra, F. I., Ahedo, E., Fife, J. M., and Martínez-Sánchez, M., "A two-dimensional hybrid model of the Hall thruster discharge," *Journal of Applied Physics*, Vol. 100, No. 2, 2006, pp. 023304.

[11] Perez-Luna, J., Hagelaar, G. J. M., Garrigues, L., and Boeuf, J. P., "Model analysis of a double-stage Hall effect thruster with double-peaked magnetic field and intermediate electrode," *Physics of Plasmas*, Vol. 14, No. 11, 2007, pp. 113502.

[12] Keidar, M., Boyd, I. D., and Beilis, I. I., "Plasma flow and plasma–wall transition in Hall thruster channel," *Physics of Plasmas*, Vol. 8, No. 12, 2001, pp. 5315–5322.

[13] Fife, J. M., "Hybrid-PIC Modeling and Electrostatic Probe Survey of Hall Thrusters," Ph.D. Thesis, Massachusetts Institute of Technology, 1998.

[14] Mikellides, I. G., Katz, I., Hofer, R. R., and Goebel, D. M., "Hall-Effect Thruster Simulations with 2-D Electron Transport and Hydrodynamic Ions," 31th International Electric Propulsion Conference, IEPC-2009-114, 2009.

[15] Kim, S.-W. and Gallimore, A. D., "Plume Study of a 1.35-kW SPT-100 Using an ExB Probe," *Journal of Spacecraft and Rockets*, Vol. 39, No. 6, 2002, pp. 904–909.

[16] Hagelaar, G. J. M., "Modelling electron transport in magnetized low-temperature discharge plasmas," *Plasma Sources Science and Technology*, Vol. 16, No. 1, 2007, pp. S57.

[17] Samuel J. Araki, R. E. W., "Magnetic Field Aligned Mesh for Ring-Cusp Discharge Chambers," 50th Joint Propulsion Conference and Exhibit, AIAA 2014-3830, 2014.

[18] Kukushkin, A., Pacher, H., Kotov, V., Pacher, G., and Reiter, D., "Finalizing the ITER divertor design: The key role of {SOLPS} modeling," *Fusion Engineering and Design*, Vol. 86, No. 12, 2011, pp. 2865 – 2873.

[19] Nishikawa, H., "A first-order system approach for diffusion equation. I: Second-order residual-distribution schemes," *Journal of Computational Physics*, Vol. 227, No. 1, 2007, pp. 315 – 352.

[20] Nishikawa, H., "A first-order system approach for diffusion equation. II: Unification of advection and diffusion," *Journal of Computational Physics*, Vol. 229, No. 11, 2010, pp. 3989 – 4016.

[21] Nishikawa, H., "First, second, and third order finite-volume schemes for advection–diffusion," *Journal of Computational Physics*, Vol. 273, No. 0, 2014, pp. 287 – 309.

[22] Chorin, A. J., "A numerical method for solving incompressible viscous flow problems," *Journal of Computational Physics*, Vol. 2, No. 1, 1967, pp. 12 – 26.

[23] Koo, J. W. and Boyd, I. D., "A mixed finite volume method for elliptic problems," *Numerical Methods for Partial Differential Equations*, Vol. 23, No. 5, 2007, pp. 1122 – 1138.

[24] Droniou, J. and Eymard, R., "A mixed finite volume scheme for anisotropic diffusion problems on any grid," *ArXiv Mathematics e-prints*, 2006.

[25] Lipnikov, K., Shashkov, M., Svyatskiy, D., and Vassilevski, Y., "Monotone finite volume schemes for diffusion equations on unstructured triangular and shape-regular polygonal meshes," *Journal of Computational Physics*, Vol. 227, No. 1, 2007, pp. 492 – 512.

[26] Kajimura, Y., Funaki, I., Matsumoto, M., Shinohara, I., Usui, H., and Yamakawa, H., "Thrust and Attitude Evaluation of Magnetic Sail by Three-Dimensional Hybrid Particle-in-Cell Code," *Journal of Propulsion and Power*, Vol. 28, No. 3, 2012, pp. 652–663.

[27] Chen, F. F. and Lieberman, M., *Introduction to plasma physics and controlled fusion*, Plenum Press, New York, 1984.

[28] Koo, J. W. and Boyd, I. D., "Modeling of anomalous electron mobility in Hall thrusters," *Physics of Plasmas*, Vol. 13, No. 3, 2006, pp. 033501.

[29] Dugan, J. J. and Sovie, R., "Volume Ion Production Costs in Tenuous Plasmas: a General Atom Theory and Detailed Results for Helium, Argon, and Cesium," NASA Technical Note, D-4150, 1967.

[30] Chen, F. F. and Lieberman, M., *Introduction to plasma physics and controlled fusion*, Vol. Chapter 5, Plenum Press, New York, 1984.

[31] Komurasaki, K. and Arakawa, Y., "Two-dimensional numerical model of plasma flow in a Hall thruster," *Journal of Propulsion and Power*, Vol. 11, No. 6, 1995, pp. 1317–1323.

[32] Rognlien, T., Milovich, J., Rensink, M., and Porter, G., "A fully implicit, time dependent 2-D fluid code for modeling tokamak edge plasmas," *Journal of Nuclear Materials*, Vol. 196 - 198, 1992, pp. 347 – 351.

[33] Harlow, F. H., Welch, J. E., et al., "Numerical calculation of time-dependent viscous incompressible flow of fluid with free surface," *Physics of fluids*, Vol. 8, No. 12, 1965, pp. 2182.

[34] Steger, J. L. and Warming, R., "Flux vector splitting of the inviscid gasdynamic equations with application to finite-difference methods," *Journal of Computational Physics*, Vol. 40, No. 2, 1981, pp. 263 – 293.

[35] Gabutti, B., "On two upwind finite-difference schemes for hyperbolic equations in non-conservative form," *Computers & Fluids*, Vol. 11, No. 3, 1983, pp. 207 – 230.

[36] Beam, R. M. and Warming, R. F., "An Implicit Factored Scheme for the Compressible Navier-Stokes Equations," *AIAA Journal*, Vol. 16, No. 4, 1978, pp. 393 – 402.

[37] Fujii, K. and Obayashi, S., "Practical applications of new LU-ADI scheme for the three-dimensional Navier-Stokes computation of transonic viscous flows," AIAA Paper, 86-0513, 1986.

[38] Weiss, J. M. and Smith, W. A., "Preconditioning applied to variable and constant density flows," *AIAA Journal*, Vol. 33, No. 11, 1995, pp. 2050–2057.

[39] Turkel, E., "Review of preconditioning methods for fluid dynamics," *Applied Numerical Mathematics*, Vol. 12, No. 1–3, 5 1993, pp. 257–284.

[40] 藤井孝藏, "流体力学の数値計算法," 東京大学出版会, 1994.

[41] Kubota, K., Funaki, I., and Okuno, Y., "Numerical Study of Plasma Behavior in a Magnetoplasmadynamic Thruster Around Critical Current," *Journal of Propulsion and Power*, Vol. 25, No. 2, 2009, pp. 397–405.

[42] Nishida, H. and Nonomura, T., "ADI-SGS scheme on ideal magnetohydrodynamics," *Journal of Computational Physics*, Vol. 228, No. 9, 2009, pp. 3182 – 3188.

[43] Powell, K. G., Roe, P. L., Linde, T. J., Gombosi, T. I., and Zeeuw, D. L. D., "A Solution-Adaptive Upwind Scheme for Ideal Magnetohydrodynamics," *Journal of Computational Physics*, Vol. 154, No. 2, 1999, pp. 284 – 309.

[44] Liou, M.-S., "A Sequel to AUSM: AUSM+," *Journal of Computational Physics*, Vol. 129, No. 2, 1996, pp. 364 – 382.

[45] Yoon, S. and Jameson, A., "Lower-upper Symmetric-Gauss-Seidel method for the Euler and Navier-Stokes equations," *AIAA Journal*, Vol. 26, No. 9, 1988, pp. 1025–1026.

[46] Lipnikov, K., Morel, J., and Shashkov, M., "Mimetic finite difference methods for diffusion equations on non-orthogonal non-conformal meshes," *Journal of Computational Physics*, Vol. 199, No. 2, 2004, pp. 589 – 597.

[47] Hofer, R. R., Peterson, P. Y., and Gallimore, A. D., "A High Specific Impulse Two-Stage Hall Thruster with Plasma Lens Focusing," 27th International Electric Propulsion Conference, IEPC-01-036, 2001.

[48] Thacker, B. H., Doebling, S. W., Hemez, F. M., Anderson, M. C., Pepin, J. E., and Rodriguez, E. A., *Concepts of model verification and validation*, No. LA-14167, Los Alamos National Laboratory, 2004.

[49] Kaneko, R., "ホールスラスタ内部のプレシースとイオン損失領域に関する数値解析," Master Thesis, The University of Tokyo, in Japanese, 2012.

[50] Cho, S., Komurasaki, K., and Arakawa, Y., "Lifetime Simulation of a SPT-Type Hall Thruster by Using a 2D Fully Kinetic PIC Model," 48th Joint Propulsion Conference and Exhibit, AIAA 2012-4016, 2012.

[51] Ahedo, E. and De Pablo, V., "Combined effects of electron partial thermalization and secondary emission in Hall thruster discharges," *Physics of Plasmas*, Vol. 14, No. 8, 2007, pp. 083501.

[52] Choueiri, E. Y., "Plasma oscillations in Hall thrusters," *Physics of Plasmas*, Vol. 8, No. 4, 2001, pp. 1411–1426.

[53] Buneman, O., "Time-reversible difference procedures," *Journal of Computational Physics*, Vol. 1, No. 4, 1967, pp. 517 – 535.

[54] Birdsall, C. K. and Langdon, A. B., *Plasma physics via computer simulation*, CRC Press, 2004.

[55] Hofer, R., Mikellides, I., Katz, I., and Goebel, D., "Wall Sheath and Electron Mobility Modeling in Hybrid-PIC Hall Thruster Simulations," 43rd Joint Propulsion Conference and Exhibit, AIAA 2007-5267, 2007.

[56] Mitrofanova, O. A., Gnizdor, R. Y., and Murashko, V. M., "New Generation of SPT-100," 32nd International Electric Propulsion Conference, IEPC-2011-041, 2011.

[57] Sommier, E., Allis, M., Gascon, N., and Cappelli, M., "Wall Erosion in 2D Hall Thruster Simulations," 42nd Joint Propulsion Conference and Exhibit, AIAA 2006-4656, 2006.

[58] Parra, F. I. and Ahedo, E., "Fulfillment of the Bohm condition on the 'HPHall' fluid-PIC code," 40th Joint Propulsion Conference and Exhibit, AIAA 2004-3955, 2004.

[59] Gamero-Castano, M. and Katz, I., "Estimation of Hall Thruster Erosion Using HPHall," 29th International Electric Propulsion Conference, IEPC-2005-303, 2005.

[60] Fife, J., Martinez-Sanchez, M., and Szabo, J., "A numerical study of low-frequency discharge oscillations in Hall thrusters," 33rd Joint Propulsion Conference and Exhibit, AIAA 1997-3052, 1997.

[61] Koizumi, H., Komurasaki, K., and Arakawa, Y., "Numerical prediction of wall erosion on a Hall thruster," *Vacuum*, Vol. 83, No. 1, 2008, pp. 67 – 71.

[62] Hara, K., Boyd, I. D., and Kolobov, V. I., "One-dimensional hybrid-direct kinetic simulation of the discharge plasma in a Hall thruster," *Physics of Plasmas*, Vol. 19, No. 11, 2012, pp. 113508.

[63] Hirano, Y., "Reduction of the Guard Erosion in a 2 Kw Anode Layer Hall Thruster," 34th International Electric Propulsion Conference, 2015.

[64] Szabo, J., "Fully Kinetic Numerical Modeling of a Plasma Thruster," Ph.D. Thesis, Massachusetts Institute of Technology, 2001.

[65] Yokota, S., "Discharge Oscillation Suppression Mechanism of a Hollow anode in a Hall Thruster," Ph.D. Thesis, The University of Tokyo, in Japanese, 2008.

[66] Cho, S., "Lifetime Investigation of Hall Thrusters by Using Multilayer Wall Probe and Plasma Particle Simulation," Ph.D. Thesis, The University of Tokyo, 2012.

[67] Miyoshi, T. and Kusano, K., "高速プラズマ流を伴う計算機シミュレーションの基礎," *J. Plasma Fusion Res.*, Vol. 83, No. 3, 2007, pp. 228 – 240.

[68] Roe, P., "Approximate Riemann solvers, parameter vectors, and difference schemes," *Journal of Computational Physics*, Vol. 43, No. 2, 1981, pp. 357 – 372.

[69] van Leer, B., "Flux-vector splitting for the Euler equations," *Eighth International Conference on Numerical Methods in Fluid Dynamics*, edited by E. Krause, Vol. 170 of *Lecture Notes in Physics*, Springer Berlin Heidelberg, 1982, pp. 507–512.

[70] Fujii, K., "有限体積法の最前線ー高速気流計算法の最近の動向," 日本計算工学会誌, Vol. 3, No. 3, 1998, pp. 158 – 166.